







Bhlhe40 and Bhlhe41 transcription factors regulate alveolar macrophage self-renewal and identity

René Rauschmeier¹, Charlotte Gustafsson², Annika Reinhardt^{3,4}, Noelia A-Gonzalez^{5,6} , Luigi Tortola⁷, Dilay Cansever⁸, Sethuraman Subramanian^{9,10,11}, Reshma Taneja¹² , Moritz J Rossner¹³ , Michael H Sieweke^{9,10,11} , Melanie Greter⁸, Robert Månsson^{2,14}, Meinrad Busslinger¹  & Taras Kreslavsky^{1,3,4,*} 

Abstract

Tissues in multicellular organisms are populated by resident macrophages, which perform both generic and tissue-specific functions. The latter are induced by signals from the microenvironment and rely on unique tissue-specific molecular programs requiring the combinatorial action of tissue-specific and broadly expressed transcriptional regulators. Here, we identify the transcription factors Bhlhe40 and Bhlhe41 as novel regulators of alveolar macrophages (AMs)—a population that provides the first line of immune defense and executes homeostatic functions in lung alveoli. In the absence of these factors, AMs exhibited decreased proliferation that resulted in a severe disadvantage of knockout AMs in a competitive setting. Gene expression analyses revealed a broad cell-intrinsic footprint of Bhlhe40/Bhlhe41 deficiency manifested by a downregulation of AM signature genes and induction of signature genes of other macrophage lineages. Genome-wide characterization of Bhlhe40 DNA binding suggested that these transcription factors directly repress the expression of lineage-inappropriate genes in AMs. Taken together, these results identify Bhlhe40 and Bhlhe41 as key regulators of AM self-renewal and guardians of their identity.

Keywords alveolar macrophages; Bhlhe40; Bhlhe41; self-renewal; tissue-resident macrophages

Subject Categories Immunology; Transcription

DOI 10.15252/embj.2018101233 | Received 25 November 2018 | Revised 18 July 2019 | Accepted 30 July 2019 | Published online 15 August 2019

The EMBO Journal (2019) 38: e101233

See also: **F Gualdrini & G Natoli** (October 2019)

Introduction

Specialized macrophages populate virtually all tissues where they provide a first line of defense against pathogens, mediate tissue homeostasis through clearance of apoptotic cells, and fulfill other, often tissue-specific, functions. The latter can be exemplified by the facilitation of pulmonary surfactant turnover by lung alveolar macrophages (AMs). While some of these tissue-resident populations, such as intestinal and dermal macrophages, are constantly replenished by circulating monocytes (Tamoutounour *et al*, 2013; Bain *et al*, 2014), other subsets, such as microglia in the brain (Ginhoux *et al*, 2010) and epidermal Langerhans cells (Merad *et al*, 2002; Hoeffel *et al*, 2012), are strictly of fetal origin and rely on local self-renewal to maintain their numbers in adulthood. A number of macrophage subsets show contribution from both fetal and adult hematopoiesis (reviewed in Ginhoux & Guillems, 2016; Perdiguero & Geissmann, 2015). This category includes peritoneal macrophages, red pulp macrophages of the spleen, liver Kupffer cells, and several other macrophage subsets. The relative contribution of adult hematopoiesis to these populations is highly age- and tissue-dependent (Sieweke & Allen, 2013; Ginhoux & Guillems, 2016).

AMs exhibit low to undetectable contribution of adult hematopoiesis in the steady state (Guillems *et al*, 2013; Gomez Perdiguero *et al*, 2014; Sawai *et al*, 2016). However, upon intranasal adoptive transfer into AM-deficient *Csf2rb*^{-/-} mice, the yolk sac-, fetal liver-, and adult bone marrow (BM)-derived precursors can all generate AMs that not only show an identical cell-surface phenotype but have extremely similar gene expression profiles irrespective of their origin (van de Laar *et al*, 2016). Similarly, AMs can be generated by adult hematopoiesis in irradiation BM chimeras. Such BM-derived AMs

1 Research Institute of Molecular Pathology (IMP), Vienna Biocenter (VBC), Vienna, Austria

2 Department of Laboratory Medicine, Center for Hematology and Regenerative Medicine, Karolinska Institutet, Stockholm, Sweden

3 Division of Immunology and Allergy, Department of Medicine Solna, Karolinska Institutet, Karolinska University Hospital, Stockholm, Sweden

4 Center for Molecular Medicine, Karolinska Institutet, Stockholm, Sweden

5 Institute of Immunology, University of Münster, Münster, Germany

6 Cells-in-Motion Cluster of Excellence (EXC 1003 – CiM), University of Münster, Münster, Germany

7 Institute of Molecular Health Sciences, ETH Zurich, Zurich, Switzerland

8 Institute of Experimental Immunology, University of Zurich, Zurich, Switzerland

9 CNRS, INSERM, CIML, Aix Marseille University, Marseille, France

10 Max-Delbrück-Centrum für Molekulare Medizin in der Helmholtzgemeinschaft (MDC), Berlin, Germany

11 Center for Regenerative Therapies Dresden (CRTD), Technische Universität Dresden, Dresden, Germany

12 Department of Physiology, Yong Loo Lin School of Medicine, National University of Singapore, Singapore City, Singapore

13 Department of Psychiatry, Molecular Neurobiology, Ludwig Maximilian University, Munich, Germany

14 Hematology Center, Karolinska University Hospital, Stockholm, Sweden

*Corresponding author. Tel: +46 8 517 761 69; E-mail: taras.kreslavsky@ki.se

exhibit dependencies on transcription factors (Schneider *et al*, 2014) and growth factors (Yu *et al*, 2017) that are indistinguishable from those of their fetal counterparts, suggesting that they differentiate along the same developmental path. These results, as well as studies of other tissue-resident macrophage populations (reviewed in Amit *et al*, 2015; Lavin *et al*, 2015), highlight an important role of the tissue microenvironment in controlling resident macrophage identity.

How exactly a given tissue microenvironment can induce the differentiation of a corresponding tissue-resident macrophage subset is an area of intense investigation, and recent studies have begun to identify signaling pathways and downstream transcription factors that regulate the differentiation of various tissue-resident macrophage populations (Lavin *et al*, 2015). For example, retinoic acid-induced expression of the transcription factor GATA6 is important for the differentiation of peritoneal macrophages (Gautier *et al*, 2014; Okabe & Medzhitov, 2014; Rosas *et al*, 2014). Likewise, the differentiation of AMs is regulated by the GM-CSF and TGF β pathways that converge on the induction of the nuclear receptor PPAR γ , which in turn induces a large part of the AM-specific transcription program (Shibata *et al*, 2001; Bonfield *et al*, 2003; Williams *et al*, 2013; Schneider *et al*, 2014; Yu *et al*, 2017). Nevertheless, it seems likely that unique properties of tissue-resident macrophages are regulated by more complex transcriptional networks rather than by the action of one or few transcription factors. Indeed, as PPAR γ is expressed by several macrophage populations including AMs and red pulp macrophages (Gautier *et al*, 2012a,b), the induction of the unique AM-specific gene expression program likely depends on cooperation with other factors.

We recently identified the two closely related basic-helix-loop-helix transcription factors Bhlhe40 (also known as Dec1, Sharp2, or Stra13) and Bhlhe41 (Dec2 or Sharp1) as key regulators of the differentiation and self-renewal of B-1a cells (Kreslavsky *et al*, 2017)—a tissue-resident innate-like B lymphocyte subset that is predominantly generated by fetal and neonatal hematopoiesis (Kreslavsky *et al*, 2018). We therefore hypothesized that these factors may also play a role in other tissue-resident self-renewing cell populations. Here, we report that AMs lacking these two transcription factors exhibited impaired proliferation that resulted in a severe disadvantage of Bhlhe40/Bhlhe41-deficient AMs in a competitive setting. In the absence of competition with wild-type (WT) cells, Bhlhe40/Bhlhe41-deficient AMs were able to maintain their numbers and displayed normal expression of the most commonly used cell-surface markers. However, genome-wide expression analysis of these Bhlhe40/Bhlhe41-deficient AMs revealed an unexpectedly broad cell-intrinsic dysregulation of the AM expression program, as indicated by the upregulation of a multitude of genes that are normally expressed in other macrophage lineages. Genome-wide profiling of Bhlhe40 binding in *ex vivo* AMs indicated that these factors may directly repress the expression of many lineage-inappropriate genes in AMs.

Results

Normal numbers and cell-surface phenotype of tissue-resident macrophages in steady-state Bhlhe40/Bhlhe41-deficient mice

To start assessing a possible role of the transcription factors Bhlhe40 and Bhlhe41 in tissue-resident macrophages, we first interrogated their expression in various macrophage populations by analyzing the Immgen Database (Heng & Painter, 2008). Expression of Bhlhe41

was restricted to AMs and microglia, while Bhlhe40 was expressed more broadly and had the highest level of expression in alveolar and peritoneal macrophages (Fig 1A). RNA flow cytometry confirmed these results at the single-cell level (Fig 1B). To test the effects of Bhlhe40 and Bhlhe41 deficiency on tissue-resident macrophages, we next compared macrophage populations in WT and Bhlhe40/Bhlhe41 double-knockout (DKO) mice. The cell-surface phenotype, frequency and numbers of alveolar, peritoneal and red pulp macrophages, as well as microglia and Kupffer cells, were normal in DKO mice compared to WT mice (Figs 1C and D, and EV1A). It was recently reported that Bhlhe40-deficient mice have a mildly reduced peritoneal macrophage compartment (Jarjour *et al*, 2019), however, when we assessed numbers of peritoneal macrophages in Bhlhe40 single KO mice we did not observe a significant change in numbers of these cells compared to WT mice (Fig EV1B). As Jarjour *et al* reported that the phenotype becomes much more pronounced upon induction of type 2 immune responses, it is conceivable that the discrepancy between our observations reflects differences in the environments of animal facilities, resulting in exposure of mice to different spectra of commensals and/or pathogens. Despite the lack of major changes in cell-surface phenotype of tissue-resident macrophages in the DKO mice, we noticed that DKO AMs expressed increased levels of CD11b (Fig 1C), a marker that is normally downregulated upon AM maturation (Schneider *et al*, 2014), and had an increased side scatter (see below).

Competitive disadvantage of Bhlhe40/Bhlhe41-deficient cells in AM compartment

We next tested if a role for Bhlhe40 and Bhlhe41 in tissue-resident macrophages could be revealed in a competitive situation. Most tissue-resident macrophages, including AMs, Kupffer cells, and peritoneal and splenic macrophages, can be reconstituted by adult hematopoiesis in irradiation BM chimeras (A-Gonzalez *et al*, 2013; Hashimoto *et al*, 2013; Bain *et al*, 2016; Scott *et al*, 2016), in line with the limited but measurable contribution of BM hematopoiesis to some of these populations in the steady state (Williams *et al*, 2013; Gomez Perdiguero *et al*, 2014; Perdiguero & Geissmann, 2015; Sawai *et al*, 2016). We therefore tested if Bhlhe40/Bhlhe41 deficiency can impact tissue-resident macrophage populations in competitive BM chimeras. To this end, a 1:1 mixture of lineage-depleted WT (CD45.1) and DKO (CD45.2) BM cells was transferred into lethally irradiated heterozygous CD45.1/CD45.2 recipients. The resulting chimeras exhibited a close to 1:1 ratio of cells of WT and DKO donor origin in the HSC-containing Lin⁻Scal⁺c-Kit⁺ (LSK) cell compartment as well as among common myeloid progenitors (CMP) and splenic monocytes (Fig 2A). However, F4/80^{hi} large peritoneal macrophages were predominantly of WT origin, and AMs were derived almost exclusively from WT donor cells in these chimeras (Fig 2A–C). Kupffer cells and F4/80^{lo} small peritoneal macrophages were also moderately biased toward the WT donor, but this effect did not reach statistical significance (Fig 2A). On the contrary, red pulp macrophages were generated more efficiently from the DKO cells (Fig 2A).

In line with the expression patterns of Bhlhe40 and Bhlhe41 (Fig 1A and B), the analysis of mixed BM chimeras generated with Bhlhe40^{-/-} or Bhlhe41^{-/-} donor cells demonstrated that AMs were affected only when both Bhlhe40 and Bhlhe41 were missing

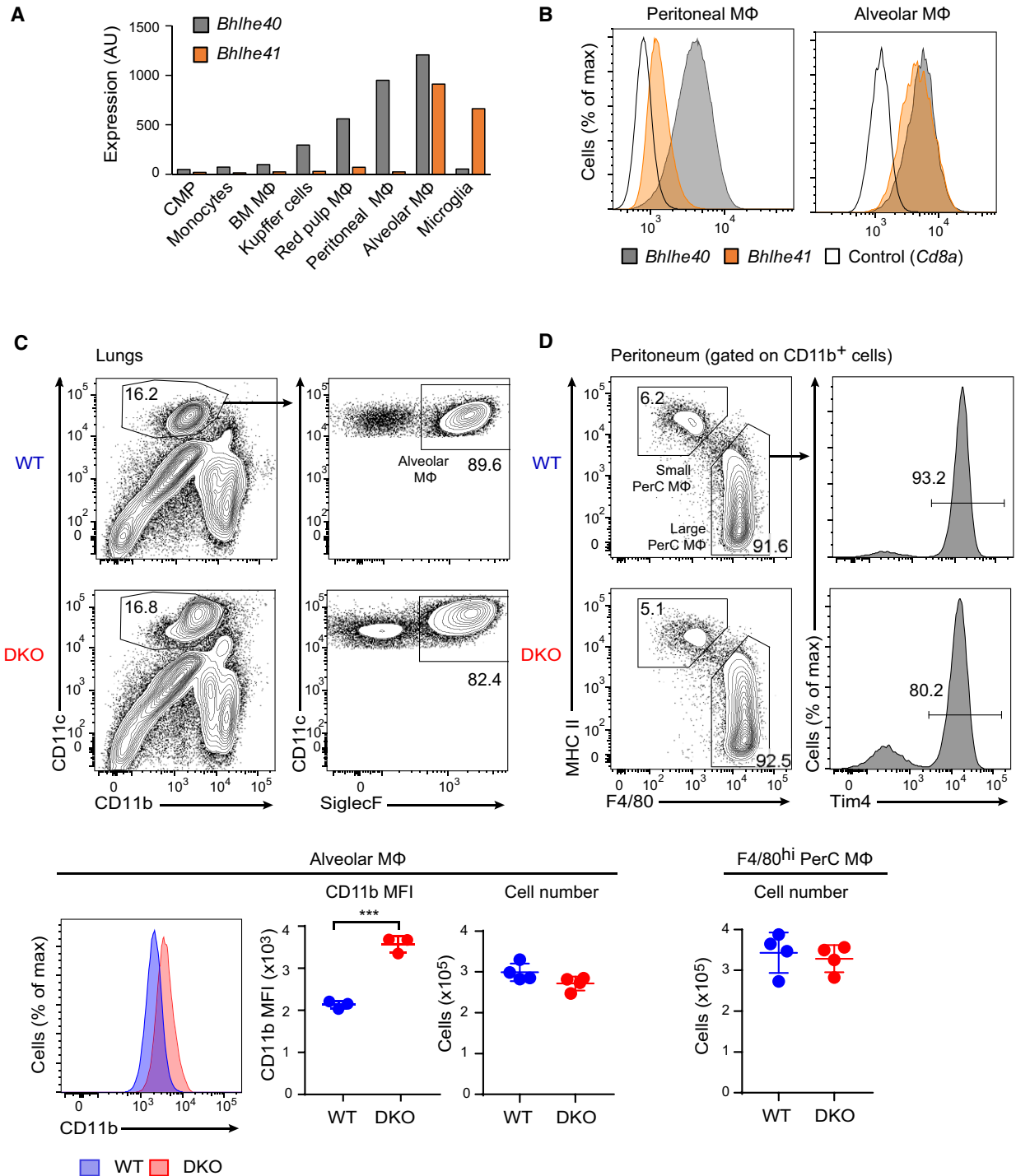


Figure 1. Expression of *Bhlhe40* and *Bhlhe41* in myeloid cells and cell-surface phenotype of DKO alveolar and peritoneal macrophages.

A Expression of *Bhlhe40* (gray) and *Bhlhe41* (orange) in the indicated cell populations, data are from the Immgen Database (microarray dataset). CMP—common myeloid progenitors. Mφ—macrophages.

B Flow cytometry detection of the *Bhlhe40* (gray) and *Bhlhe41* (orange) transcripts by the PrimeFlow RNA assay in alveolar (right) and peritoneal (left) macrophages. A probe specific for the *Cd8a* mRNA (black line) was used as a negative control. Results are representative of at least four independent experiments.

C, D Cell-surface phenotype and numbers of alveolar (C; digested lung) and peritoneal (D) macrophages in WT and DKO mice. Additional gating for CD11b⁺ cells was applied for peritoneal macrophages as indicated. Levels of CD11b expression on WT and DKO AMs are shown, and median fluorescent intensity for CD11b expression was quantified (C, bottom left; three mice per genotype). Absolute numbers of CD11c^{hi}CD11b^{lo}SiglecF^{hi} alveolar macrophages from digested lungs (C) and CD11b⁺F4/80^{hi} peritoneal macrophages (D) from WT and DKO mice are shown (bottom; four mice per genotype). Representative results of two independent experiments. Horizontal lines indicate the mean and error bars represent s.d. ****P* < 0.001 (Student's *t*-test).

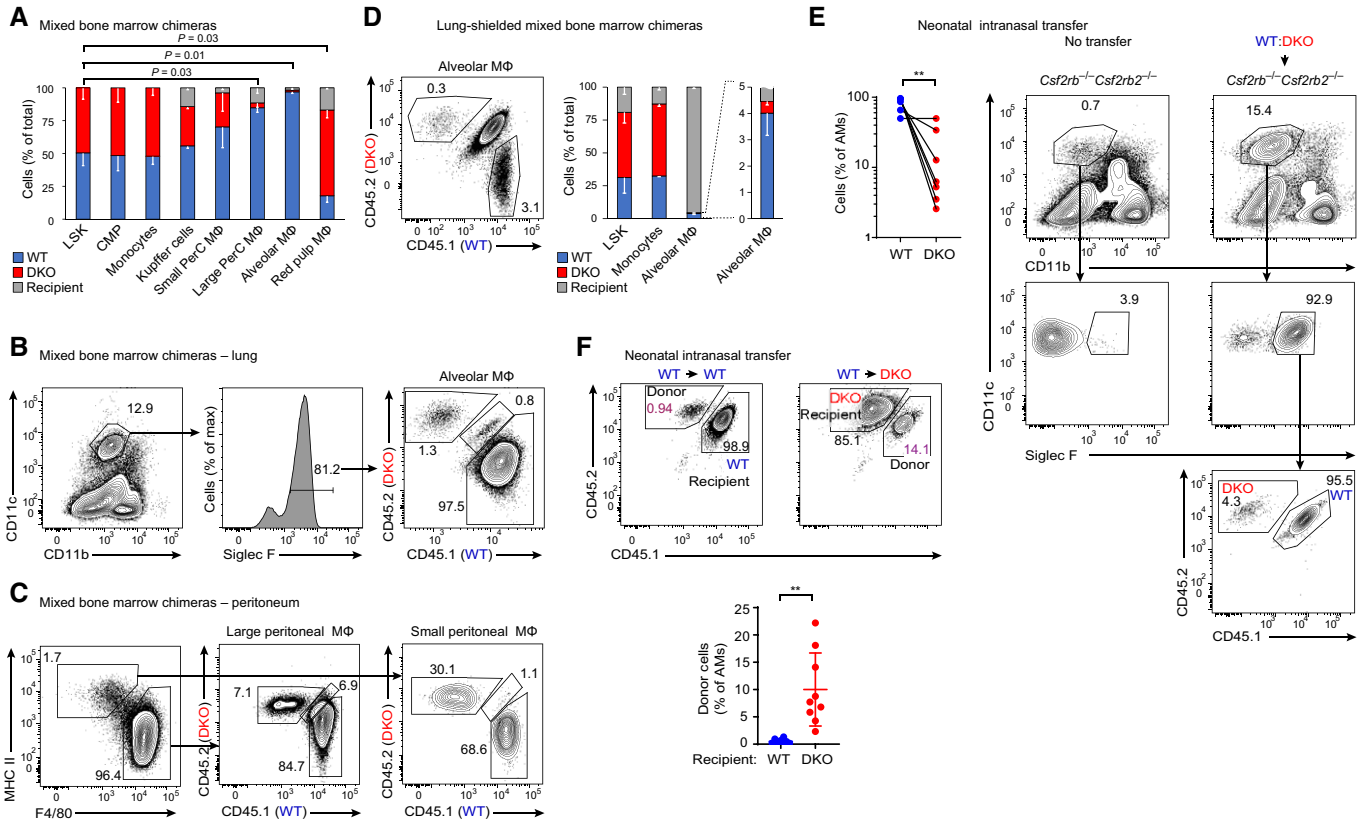


Figure 2. Competitive disadvantage of Bhlhe40/Bhlhe41-deficient cells in AM compartment.

A Frequency of WT donor (CD45.1), and DKO donor (CD45.2) and recipient (CD45.1/2) cells in the indicated BM (LSK, CMP), splenic (monocytes and red pulp macrophages), liver (Kupffer cells), peritoneal and alveolar macrophage populations of lethally irradiated recipients ≥ 6 weeks after transfer of a 1:1 mixture of lineage-depleted BM cells from WT and DKO mice. P values < 0.05 (paired Student's t -test) between LSK and other populations are shown for frequencies of WT cells. Three mixed BM chimeras were analyzed; error bars represent s.d. Representative results of three independent experiments.

B, C Representative flow cytometric analysis of lung (B) and peritoneal (C) macrophages as in (A) (left). The expression of CD45.1 and CD45.2 on donor and recipient cells is shown next to the indicated gates (right).

D Frequency of WT donor (CD45.1), and DKO donor (CD45.2) and recipient (CD45.1/2) cells among the BM LSK cells, splenic monocytes, and alveolar macrophages of the recipients that were irradiated with lung shielding, treated with one dose of busulfan as described in Materials and Methods, transferred with a 1:1 mixture of lineage-depleted BM cells from WT and DKO mice, and analyzed ≥ 8 weeks after transfer. Representative flow cytometry results for alveolar macrophages (left) and quantification (right) is shown. Single experiment with three chimeras. Error bars represent s.d.

E Surface phenotype of cells from the digested lungs (right) and quantification of donor contribution to the AM compartment (left) of AM-deficient $Csf2rb^{-1}Csf2rb2^{-1}$ recipients (CD45.2) that were subjected to intranasal transfer of a 1:1 mixture of sorted fetal liver monocytes from WT (CD45.1/2) and DKO (CD45.2) E18.5 embryos at days 1 or 2 after birth and analyzed ≥ 7 weeks after the transfer. Cell-surface phenotype of lung cells from a $Csf2rb^{-1}Csf2rb2^{-1}$ mouse that was not subjected to the transfer is shown for comparison. Single experiment with seven recipients. $**P < 0.01$ (paired Student's t -test).

F Frequency of donor- and recipient-derived AMs in WT and DKO recipients transferred at days 1 or 2 after birth intranasally with WT CD45⁺ cells sorted from neonatal lungs and analyzed ≥ 7 weeks after the transfer. Results for quantification (lower panel) are pooled from three independent experiments with a total of eight WT and nine DKO recipients; various combinations of CD45.1 and CD45.2 were used to distinguish donor and recipient cells. Horizontal lines indicate the mean and error bars represent s.d. $**P < 0.01$ (Student's t -test).

(Fig EV1C and D). These results are consistent with the redundancy between Bhlhe40 and Bhlhe41 observed in other systems (Rossner *et al*, 2008; Shahmoradi *et al*, 2015; Kreslavsky *et al*, 2017). In contrast, the Bhlhe40 deficiency was solely responsible for the competitive disadvantage in peritoneal macrophages (Fig EV1C and D), in line with a recent report (Jarjour *et al*, 2019).

Full-body irradiation can cause damage to lung tissue that could potentially alter properties of the resident phagocytes. To test if Bhlhe40/Bhlhe41 deficiency affects AM competitiveness when such damage is limited, we next performed mixed BM chimera

experiments using recipients, whose lungs were shielded during irradiation. To allow for some reconstitution of the AM compartment, these recipients were treated with a single low dose of chemotherapeutic drug busulfan (Hubbard *et al*, 2008). Eight weeks after the reconstitution, the recipient mice exhibited a high contribution of both WT and DKO donor cells to the hind leg BM LSK compartment as well as to splenic monocytes (Fig 2D). In contrast, AMs remained largely of the recipient origin with only 3–5% contribution of donor cells. These rare donor-derived AMs, however, were predominantly of WT origin (Fig 2D). Thus, Bhlhe40/Bhlhe41

deficiency results in a competitive disadvantage of AMs in mixed BM chimeras even when the damage to the lung tissue is limited.

The observations described above clearly demonstrate that adult hematopoietic cells that lack *Bhlhe40* and *Bhlhe41* fail to contribute to the AM compartment efficiently in the presence of WT competitor cells. However, at the steady-state situation, the majority of AMs in adult mice are of fetal origin. To test if *Bhlhe40* and *Bhlhe41* are also required for competitive fitness of fetal-derived AMs, we next took advantage of the observation that intranasal transfer of AM precursors into neonatal mice with a defective AM compartment, but not into WT mice, can result in efficient engraftment of the transferred cells (Schneider *et al*, 2014; van de Laar *et al*, 2016). We first used neonatal GM-CSF receptor knockout (*Csf2rb*^{-/-}/*Csf2rb2*^{-/-}) mice, that lack AMs, as recipients, transferred intranasally a 1:1 mixture of sorted fetal liver monocytes from WT (CD45.1/CD45.2 heterozygous) and DKO (CD45.2) embryos and analyzed the mice ≥ 7 weeks after reconstitution. As expected, untransferred control mice did not have any cells with a CD11c⁺ Siglec F⁺ AM phenotype in the lungs (Fig 2E). Intranasal transfer resulted in reconstitution of the AM compartment, and AMs were predominantly of WT origin (Fig 2E). In a complementary approach, we tested if the AM defect caused by the absence of *Bhlhe40* and *Bhlhe41* rendered the neonatal DKO mice themselves receptive to intranasal transfer of WT AM precursors. To this end, we transferred equal numbers of WT hematopoietic cells sorted from neonatal lungs intranasally into congenically distinguishable WT and DKO neonates and analyzed these mice ≥ 7 weeks after transplantation. While only $0.32 \pm 0.19\%$ contribution of donor cells to the AM compartment was observed in WT recipients, $10.6 \pm 7.3\%$ of donor cells were detected in DKO recipients (Fig 2F). Importantly, we did not observe alterations in the composition of the lung myeloid compartment of neonatal DKO mice (Fig EV1D), suggesting that the increased engraftment of transferred cells was not due to a decreased abundance of AM precursors in the DKO recipients. Taken together, these experiments demonstrate that inability of DKO AMs to compete against their WT counterparts is not restricted to cells generated by adult hematopoiesis and also applies to AMs of fetal origin. These results further support the notion that a competitive disadvantage of DKO AMs can be observed in the absence of irradiation-induced lung damage.

Regulation of AM proliferation by *Bhlhe40* and *Bhlhe41*

We next aimed to identify the mechanisms underlying the competitive disadvantage of the DKO macrophages. As a recent report attributed competitive disadvantage of *Bhlhe40*^{-/-} peritoneal macrophages to their impaired proliferation (a phenotype that required induction of the type 2 immune response to be clearly detected; Jarjour *et al*, 2019), we focused our analysis on AMs. DKO AMs did not show an increase in apoptosis (data not shown), but in mixed BM chimeras exhibited reduced proliferation, as judged by a twofold decrease in EdU incorporation (Fig 3A). These results suggested that the competitive disadvantage of DKO AMs in chimeras can, at least in part, be explained by their impaired proliferation. To test if this defect can only be observed in AMs of BM origin, we next compared EdU incorporation by AMs in unmanipulated WT and DKO mice. These experiments again demonstrated a twofold decrease in the proliferation of DKO AMs (Fig 3B and C).

Moreover, when CellTrace Violet-labeled WT and DKO AMs were co-cultured in the presence of GM-CSF, DKO cells again exhibited impaired proliferation and were rapidly outcompeted by WT AMs (Fig 3D), while the extent of cell death was identical in cultured WT and DKO AMs (Fig EV2A). We conclude that DKO AMs exhibit a decrease in proliferation that results in a severe disadvantage of these cells under competitive conditions.

To begin the characterization of the molecular mechanisms underlying the defective proliferation of DKO AMs, we next compared their gene expression profiles to that of WT AMs by RNA-seq. These experiments revealed the downregulation of many proliferation-associated genes in DKO AMs (Fig EV2B). A similar downregulation was observed in DKO peritoneal macrophages (Fig EV2B), confirming the recently published observations made for *Bhlhe40*-deficient peritoneal macrophages (Jarjour *et al*, 2019). It was previously suggested that the low expression of the transcription factors *Maf* and *Mafb*, which function as negative regulators of macrophage proliferation (Aziz *et al*, 2009), contributes to the self-renewal capacity of AMs (Soucie *et al*, 2016). Consistent with the low proliferative rate of DKO AMs, *Maf* and *Mafb* were strongly upregulated in the DKO AMs both in the steady state and in mixed BM chimeras (Fig 3E). Interestingly, the expression of previously reported *Maf*/*Mafb*-repressed self-renewal associated target genes (*Myc*, *Klf2*, *Klf4*; Soucie *et al*, 2016) was not significantly changed in DKO AMs (data not shown), suggesting that *Maf* and *Mafb* regulate the proliferation of AMs via additional regulatory circuits. We conclude that the impaired self-renewal-associated proliferation of DKO AMs is associated with increased expression of *Maf* and *Mafb*, two negative regulators of macrophage self-renewal.

Accumulation of lipids in AMs in the absence of *Bhlhe40* and *Bhlhe41*

We next sought to test whether *Bhlhe40*/*Bhlhe41*-deficient AMs are functionally normal. A key function of AMs is the facilitation of pulmonary surfactant turnover (Garbi & Lambrecht, 2017), and the impaired function of AMs in many knockout strains is manifested by the accumulation of lipid droplets in these cells—a phenotype that is thought to reflect their impaired ability to catabolize lipid-rich surfactant (Baker *et al*, 2010; Schneider *et al*, 2014; Suzuki *et al*, 2014; Yu *et al*, 2017). Oil Red O staining of cytopun cells from bronchoalveolar lavages (BAL) revealed the presence of cells with a high lipid droplet content in DKO but not WT mice (Fig 4A and B). We also noticed that AMs in DKO mice exhibited an increase in side scatter (SSC), a parameter that reflects the internal complexity of a cell (Fig 4C, middle). To test if these alterations also reflect the accumulation of lipids, we performed staining with the lipophilic dyes BODIPY 493/503 (Fig 4C) and Nile Red (not shown). The staining closely reflected the side scatter but not forward scatter characteristics of the cells, and DKO cells exhibited both an overall increase in staining and emergence of SSC^{hi}BODIPY^{hi} cells (Fig 4C). We conclude that, despite their normal numbers, AMs in *Bhlhe40*/*Bhlhe41*-deficient mice may be functionally impaired, as evidenced by the accumulation of lipids in these cells. This dysfunction of AMs in DKO mice did, however, not result in the development of alveolar proteinosis that is observed in mice with a complete block in AM differentiation (Dranoff *et al*, 1994; Williams *et al*, 2013; Schneider *et al*, 2014; Suzuki *et al*, 2014; Yu *et al*, 2017), as judged by the

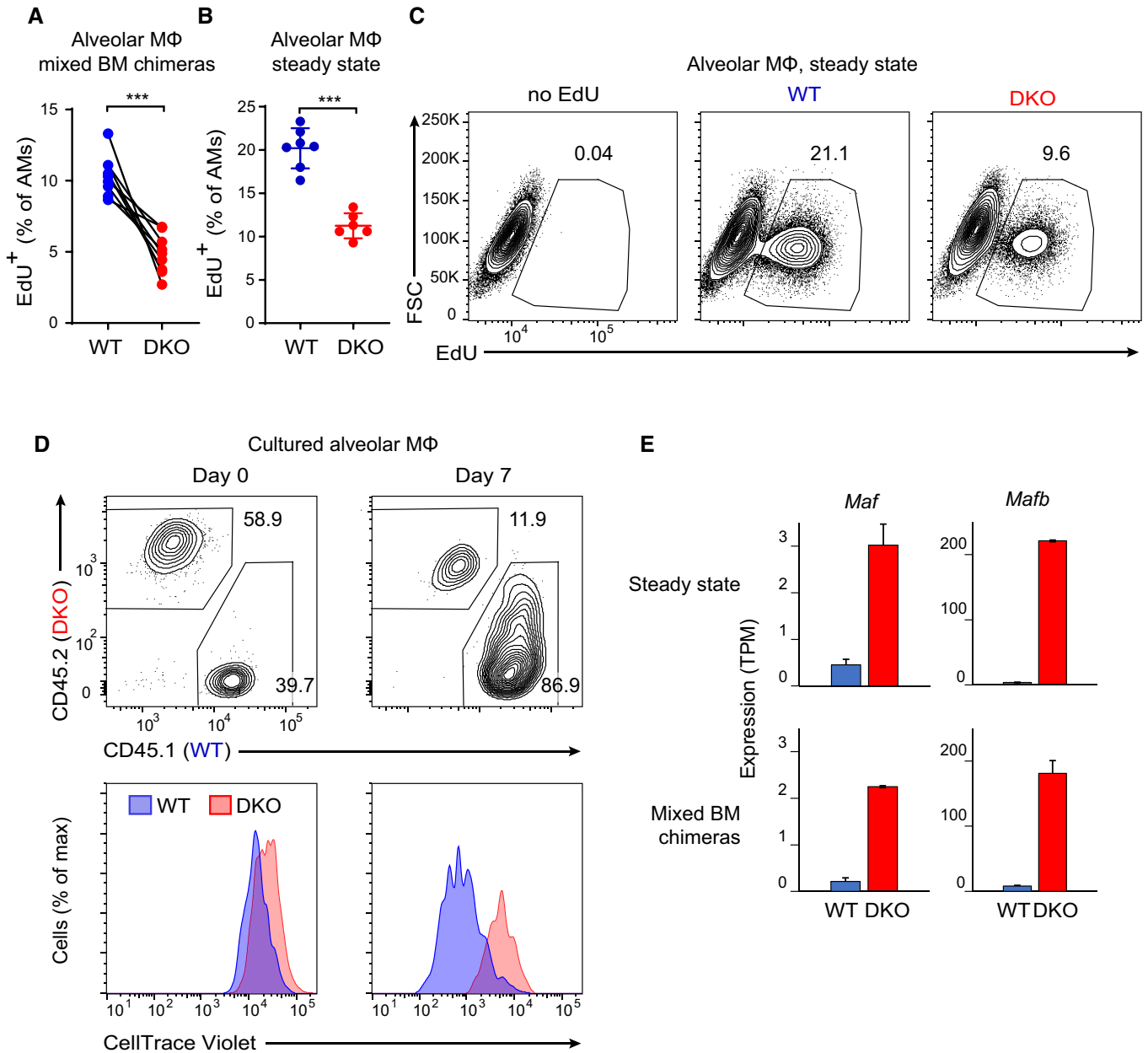


Figure 3. Impaired proliferation of DKO AMs.

A Mixed WT:DKO BM chimeras established as in Fig 2A were injected with EdU on three consecutive days. EdU incorporation was analyzed 1 day after the last injection. Results pooled from two independent experiments; nine BM chimeras were analyzed in total. ****P* < 0.001 (Student's *t*-test).

B, C Steady-state WT and DKO mice were injected with EdU and analyzed as in (A). Representative flow cytometry plots of EdU incorporation by AMs (C) and their quantification (results pooled from two independent experiments, seven WT and six DKO mice were analyzed in total) (B) are shown. Horizontal lines indicate the mean, error bars represent s.d. ****P* < 0.001 (Student's *t*-test).

D WT (CD45.1) and DKO (CD45.2) AMs were sorted, mixed in a 1:1 ratio, labeled with CellTrace Violet, and cultured in the presence of GM-CSF. The ratio of CD45.1 and CD45.2 cells and CellTrace Violet dilution was analyzed prior to culture (day 0) and after 7 days of culture as described in Materials and Methods. Results representative of two independent experiments.

E RNA-seq analysis of *Maf* and *Mafb* expression in WT and DKO AMs, which were isolated by flow cytometry from mice in steady state (top) or from mixed BM chimeras (bottom). Error bars represent s.e.m.; two biological replicates per genotype.

normal levels of surfactant pulmonary associated protein D in BAL of DKO mice (Fig EV2C).

To test if the accumulation of lipids by DKO AMs could be rescued by the presence of WT AMs, we compared the lipid content

of WT and DKO AMs in mixed BM chimeras. As the numbers of DKO AMs are very scarce in this setting, we utilized flow cytometry to analyze the lipid droplet content by staining AMs from chimeras with BODIPY. In this setting, no increase in BODIPY staining or side

scatter could be detected for DKO AMs (Fig 4D and data not shown). This result is reminiscent of a much less pronounced accumulation of lipid droplets in PPAR γ -deficient AMs in a mixed BM chimera setting compared to that observed in the steady state (Schneider *et al*, 2014). These results can have two alternative explanations: either the observed accumulation of lipid droplets in AMs of DKO mice is caused solely by cell-extrinsic factors, or a cell-intrinsic defect in processing of lipid-rich surfactant by DKO AMs is masked in mixed BM chimeras by efficient clearing of old surfactant by the abundant WT AMs. While future functional studies will be required to directly test these possibilities, we checked if our RNA-seq comparison of WT and DKO AMs may provide some evidence for one of these hypotheses. We focused our analysis on the genes that were downregulated in DKO AMs in a cell-intrinsic fashion both at steady state and in mixed BM chimeras. These DKO-downregulated genes were enriched in genes encoding factors involved in very long-chain fatty acid metabolic processes (GO:0000038; $P = 0.002$; *Acot4*, *Cyp4f18*, *Hsd17b4*) and lipid metabolic processes (GO:0006629; $P = 0.059$; *Acap1*, *Acaa1b*, *Hsd17b4*, *Hsd11b1*, *Lpcat4*, *Pnpla5*) (DAVID functional annotation tool; Huang *et al*, 2008). This included the downregulation of genes encoding two enzymes important for fatty acid β -oxidation—acetyl-coenzyme A acyltransferase 1B (*Acaa1b*) and hydroxysteroid 17-beta dehydrogenase 4 (*Hsd17b4*; Fig 4E) that were also downregulated in PPAR γ -deficient lung macrophages, possibly contributing to lipid droplet accumulation in these cells (Schneider *et al*, 2014). Thus, while lipid accumulation in DKO AMs can be rescued by the presence of WT AMs, DKO macrophages exhibit a cell-intrinsic downregulation of genes encoding factors involved in lipid metabolism.

Regulation of *Bhlhe40* and *Bhlhe41* expression in AM development

To test when *Bhlhe40* and *Bhlhe41* are induced in AM differentiation, we assessed the expression of these genes in myeloid cells from embryonic day 17.5 (E17.5) livers and lungs, as well as from postnatal day 2 (P2) and adult lungs by RNA flow cytometry (Fig EV3A and B). Ly6c^{hi} monocytes of fetal liver origin are thought to colonize the lung during late embryonic development and, after Ly6c downregulation and progression through a transitional pre-AM stage, give rise to cells with a mature CD11c^{hi}Siglec F^{hi} AM phenotype after birth (Guilliams *et al*, 2013). Our RNA flow cytometry analysis demonstrated that, while fetal liver monocytes were uniformly *Bhlhe40* negative or low, this gene was upregulated and showed a broad range of expression levels in monocytes from fetal lungs, with *Bhlhe40*-negative cells being confined within a fraction of cells with the highest levels of Ly6c expression (Fig EV3A). In contrast, myeloid cells expressing high levels of *Bhlhe41* were absent from E17.5 lungs and only emerged at P2. Expression of this factor coincided with upregulation of CD11c and Siglec F and was restricted to cells that upregulated these markers (Fig EV3A and B). These results demonstrate that *Bhlhe40* is induced already in fetal monocytes, possibly upon their entry into the lung, while *Bhlhe41* upregulation occurs at late stages of AM differentiation and coincides with acquisition of a mature AM cell-surface phenotype.

To identify pathways that may contribute to *Bhlhe40* and *Bhlhe41* upregulation in developing AMs, we performed analysis of publicly available gene expression profiles of AMs mutant for *Pparg* (Schneider *et al*, 2014), *Csf2rb* (Suzuki *et al*, 2014), and *Tgfb2* (Yu *et al*, 2017).

Pparg and *Csf2rb* deficiency did not alter *Bhlhe40* and *Bhlhe41* expression (Fig EV3C), indicating that PPAR γ and GM-CSF signaling were dispensable for the expression of these factors by lung macrophages. On the contrary, *Itgax*^{Cre} *Tgfb2*^{fl/fl} AMs exhibited a moderate reduction in *Bhlhe40* and *Bhlhe41* expression compared to their WT counterparts (Fig EV3C). Of note, these changes may underestimate the role of TGF- β signaling in *Bhlhe40*/*Bhlhe41* activation, as only 60% *Tgfb2* deletion was observed in AMs in *Itgax*^{Cre} *Tgfb2*^{fl/fl} mice (Yu *et al*, 2017). We next tested if TGF- β signaling is sufficient to induce *Bhlhe40* and *Bhlhe41* upregulation in fetal liver monocytes *in vitro*. A 24-h treatment with TGF- β 1 resulted in a mild but significant upregulation of *Bhlhe40* but not *Bhlhe41* in cultured fetal liver monocytes when compared to cells cultured in the presence of a blocking anti-TGF- β 1 antibody (Fig EV3D). Taken together, these results are consistent with a model in which *Bhlhe40* is upregulated already in fetal monocytes—possibly upon their first exposure to the lung microenvironment and activation of TGF- β signaling, while *Bhlhe41* upregulation occurs during late stages of AM differentiation.

Broad footprint of *Bhlhe40*/*Bhlhe41* deficiency on the AM transcriptome

Detailed comparison of the RNA-seq expression data of WT and DKO AMs revealed an unexpectedly broad footprint of *Bhlhe40*/*Bhlhe41* deficiency, with 957 genes being significantly upregulated and 591 genes significantly downregulated in DKO AMs (> 2-fold, adjusted $P < 0.05$; Appendix Fig S1A). A similar analysis of WT and DKO peritoneal macrophages identified only 311 upregulated and 281 downregulated genes (Appendix Fig S1A). Comparison of the differentially regulated genes indicated that the *Bhlhe40*/*Bhlhe41* transcription factors regulate partially overlapping but largely distinct expression programs in the two macrophage populations (Appendix Fig S1B).

The extensive change in gene expression in AMs of the DKO mice, carrying germline mutations in *Bhlhe40* and *Bhlhe41*, could be caused by non-cell-intrinsic mechanisms. It was also conceivable that, due to the self-renewal defect of DKO AMs, these cells may have been replaced by macrophages of BM origin and, in such a scenario, the gene expression changes could reflect a difference in the origin of the cells. To address these possibilities, we again took advantage of the mixed BM chimera approach, as adult BM-derived monocytes can give rise to AMs with gene expression profiles very similar to that of fetal-derived AMs (van de Laar *et al*, 2016). As DKO AMs had a severe competitive disadvantage in mixed BM chimeras (Fig 2A and B), we mixed WT and DKO BM cells at a 1:20 ratio to obtain sufficient DKO AMs for RNA-seq analysis. Even under these conditions, DKO cells represented only 6–7% of total AMs (Appendix Fig S1C), further highlighting the extremely poor ability of the DKO AMs to compete against their WT counterparts. In this setting, few DKO AMs were therefore residing in the lung of WT recipient mice that were largely “serviced” by WT AMs of both donor and recipient origin. Comparison of WT and DKO donor-derived AMs by RNA-seq revealed gene expression changes that correlated well with those observed in steady-state DKO AMs (Fig 5A; Pearson correlation coefficient 0.715). These results indicated that most of the observed changes in the transcriptome of AMs resulted from cell-intrinsic effects of *Bhlhe40*/*Bhlhe41* deficiency. Moreover, as these changes were observed in mixed BM

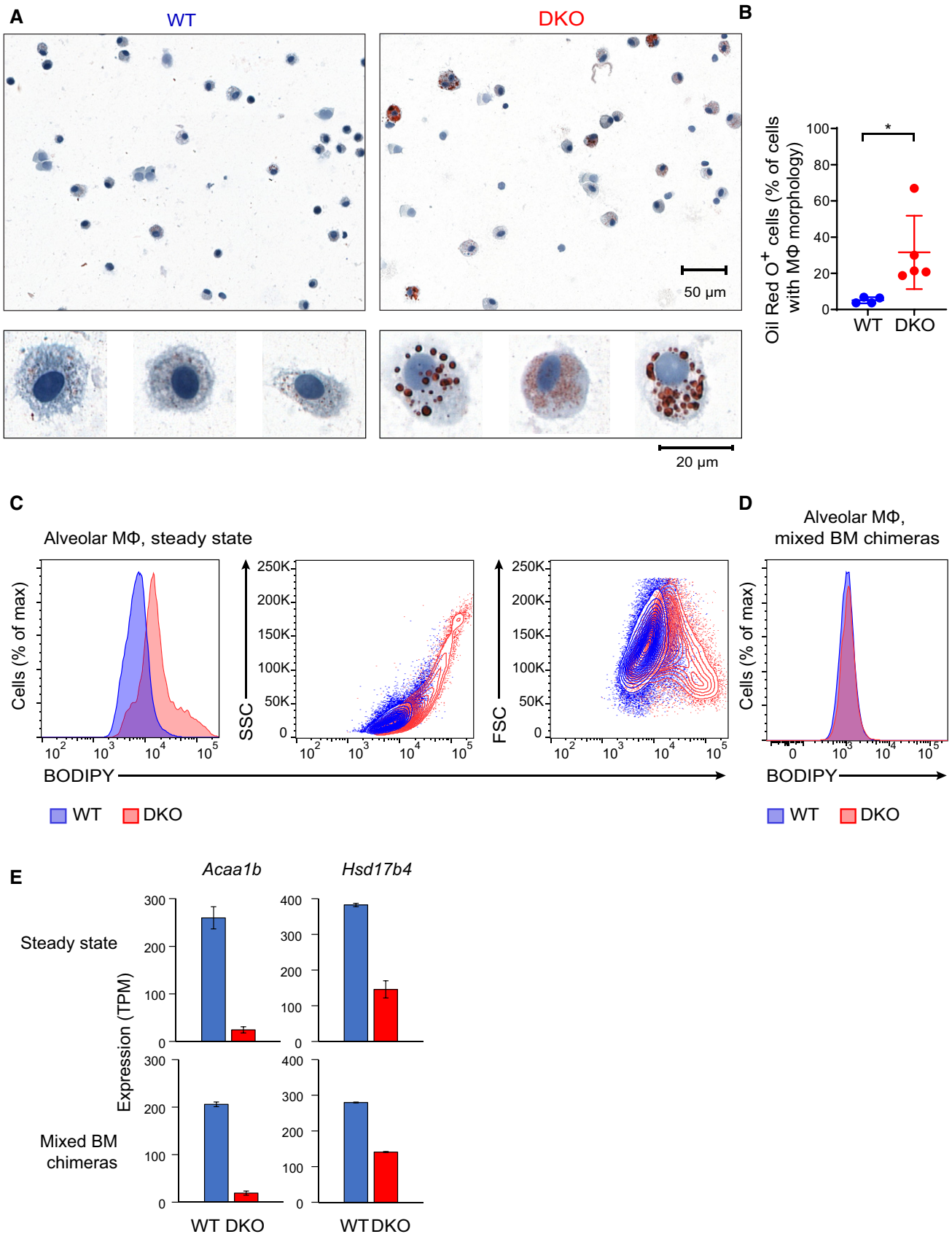


Figure 4.

Figure 4. Accumulation of lipids in AMs of DKO mice.

- A Staining of bronchoalveolar lavage cytopsin from WT and DKO mice with the lipophilic dye Oil Red O. Representative results of two independent experiments.
- B Quantification of Oil Red O-positive cells in WT and DKO mice for individual animals. Horizontal lines indicate the mean and error bars represent s.d. * $P < 0.05$ (Student's t -test). Results pooled from two independent experiments; four WT and five DKO mice were analyzed in total.
- C Flow cytometric analysis of AMs from WT and DKO mice stained with the lipophilic dye BODIPY 493/503. Representative results of two independent experiments with three mice per group.
- D Analysis as in (C) performed with WT:DKO mixed BM chimeras. Gating on CD45.1 and CD45.2 was applied to identify cells of WT and DKO donor origin. Representative results of two independent experiments with at least three chimeras.
- E RNA-seq analysis of *Acaa1b* and *Hsd17b4* expression in WT and DKO AMs, which were isolated by flow cytometry from mice in steady state (top) or from mixed BM chimeras (bottom). Error bars represent s.e.m.; two biological replicates per genotype.

chimeras where both WT and DKO macrophages originate from BM-derived monocytes, these gene expression changes did not reflect differences in macrophage origin. To focus strictly on the cell-intrinsic effects of Bhlhe40/Bhlhe41 deficiency, we restricted most of the subsequent analyses to genes that exhibited significant changes in the same direction both in steady state and in BM chimeras.

We next tested if the broad changes in gene expression in DKO AMs might be explained by differences in the expression of known AM regulators. Genes encoding signaling molecules of the GM-CSF and TGF- β pathways, the nuclear receptor PPAR γ and its heterodimerization partners of the retinoid X receptor (RXR) family, or the transcription factors Bach2, Zeb2, and C/EBP β were not downregulated in DKO AMs (Fig 5A), indicating that Bhlhe40 and Bhlhe41 do not execute their function in AMs by inducing the expression of these factors.

To identify genes that are likely to be directly regulated by the transcription factors Bhlhe40 and Bhlhe41, we utilized an optimized tagmentation-based ChIP protocol (Gustafsson *et al*, 2019) that allowed us to map genome-wide binding of Bhlhe40 directly in *ex vivo* AMs (Figs 5B and EV4A). Peak calling with a stringent P value of $< 10^{-10}$ identified 12,740 Bhlhe40-binding regions, and assignment of the peaks to the nearest gene within a 50-kb window defined 6,517 Bhlhe40 target genes (data not shown). *De novo* motif discovery identified the CACGTG version of the E-box (Fig 5C) that we and others previously described as the Bhlhe40/Bhlhe41 binding motif (Jolma *et al*, 2013; Kreslavsky *et al*, 2017). Almost half of the Bhlhe40-binding sites were observed within gene bodies, whereas only 28% of the binding sites were present in intergenic regions (Fig 5D).

It was previously reported that Bhlhe40 and Bhlhe41 function predominantly as transcriptional repressors in many (Ow *et al*, 2014) but possibly not all (Numata *et al*, 2018) cellular contexts. In line with the repressive function of these transcription factors in AMs, gene set enrichment analysis (GSEA) demonstrated that genes associated with Bhlhe40 peaks were enriched among genes upregulated in DKO AMs (Figs 5E and EV4B). Stratification of Bhlhe40 peaks by their P values indicated that this enrichment was particularly pronounced for genes in the vicinity of high-ranking Bhlhe40 peaks (Fig 5E) but remained significant even for the low-scoring peaks (Fig EV4B). Accordingly, genes upregulated in the DKO AMs were more frequent among those that had Bhlhe40 binding in their vicinity and this increase was again more prominent for high-ranking Bhlhe40 peaks (Fig EV4C). On the contrary, the frequency of genes downregulated in DKO AMs was not significantly influenced by presence or absence of Bhlhe40 binding (Fig EV4C). While

this analysis cannot fully exclude a possible activating role of Bhlhe40/Bhlhe41 at some loci, it suggests that the major function of these transcription factors in AMs is transcriptional repression.

It was previously suggested that Bhlhe40 and Bhlhe41 repress gene expression at least in part through recruitment of histone deacetylases (HDACs; Sun & Taneja, 2000; Garriga-Canut *et al*, 2001; Kato *et al*, 2014; Ow *et al*, 2014)—but genome-wide effects of the ablation of these transcription factors on histone acetylation were, to our knowledge, not assessed to date in any cell type. We therefore compared H3K27 acetylation (H3K27ac) in *ex vivo* WT and DKO AMs by ChIP-seq. Many regulatory elements that exhibited Bhlhe40 binding showed an increase in H3K27 acetylation in DKO AMs (Figs 5B and F, and EV4A and D). The frequency of regions with increased H3K27 acetylation in DKO AMs was higher for regulatory elements that exhibited Bhlhe40 binding than for those that did not have a Bhlhe40 peak in their close proximity (AM ATAC-seq peaks (Yoshida *et al*, 2019), see Materials and Methods for details) (Figs 5F and EV4D). In line with the effects of Bhlhe40 binding on gene expression described above, increased H3K27 acetylation in DKO AMs was most pronounced at the regulatory elements associated with the high-ranking Bhlhe40 peaks (Figs 5F and EV4D). We conclude that Bhlhe40 binding is associated with a decrease in H3K27 acetylation at a subset of the binding sites.

Genes encoding the negative regulators of macrophage proliferation, *Maf* and *Mafb*, that were upregulated in DKO AMs, were located 196 kb (*Maf*) and 53 kb (*Mafb*) away from the nearest Bhlhe40 peaks. Additional strong Bhlhe40 peaks were detected 279 and 156 kb downstream of *Maf* and *Mafb*, respectively, and Bhlhe40/Bhlhe41 deficiency resulted in increased H3K27 acetylation of these regulatory elements in AMs (Fig EV4E). It remains to be tested if Bhlhe40/Bhlhe41 repress *Maf* and *Mafb* genes through these distant enhancers or by an indirect mechanism.

Taken together, these results show an unexpectedly broad cell-intrinsic footprint of Bhlhe40/Bhlhe41 deficiency on the transcriptome of AMs and suggest that some of this regulation happens through direct repression of genes by these transcription factors, likely occurring at least in part through histone deacetylation.

Bhlhe40 and Bhlhe41 regulate AM identity

While DKO AMs exhibited normal expression of the most commonly used AM cell-surface markers, with the exception of the mild upregulation of CD11b (Fig 1C), the broad transcriptional footprint of Bhlhe40/Bhlhe41 deficiency prompted us to analyze the expression of the AM signature genes in these cells. To this end, we utilized the “AM signature” and “non-AM macrophage signature” gene sets

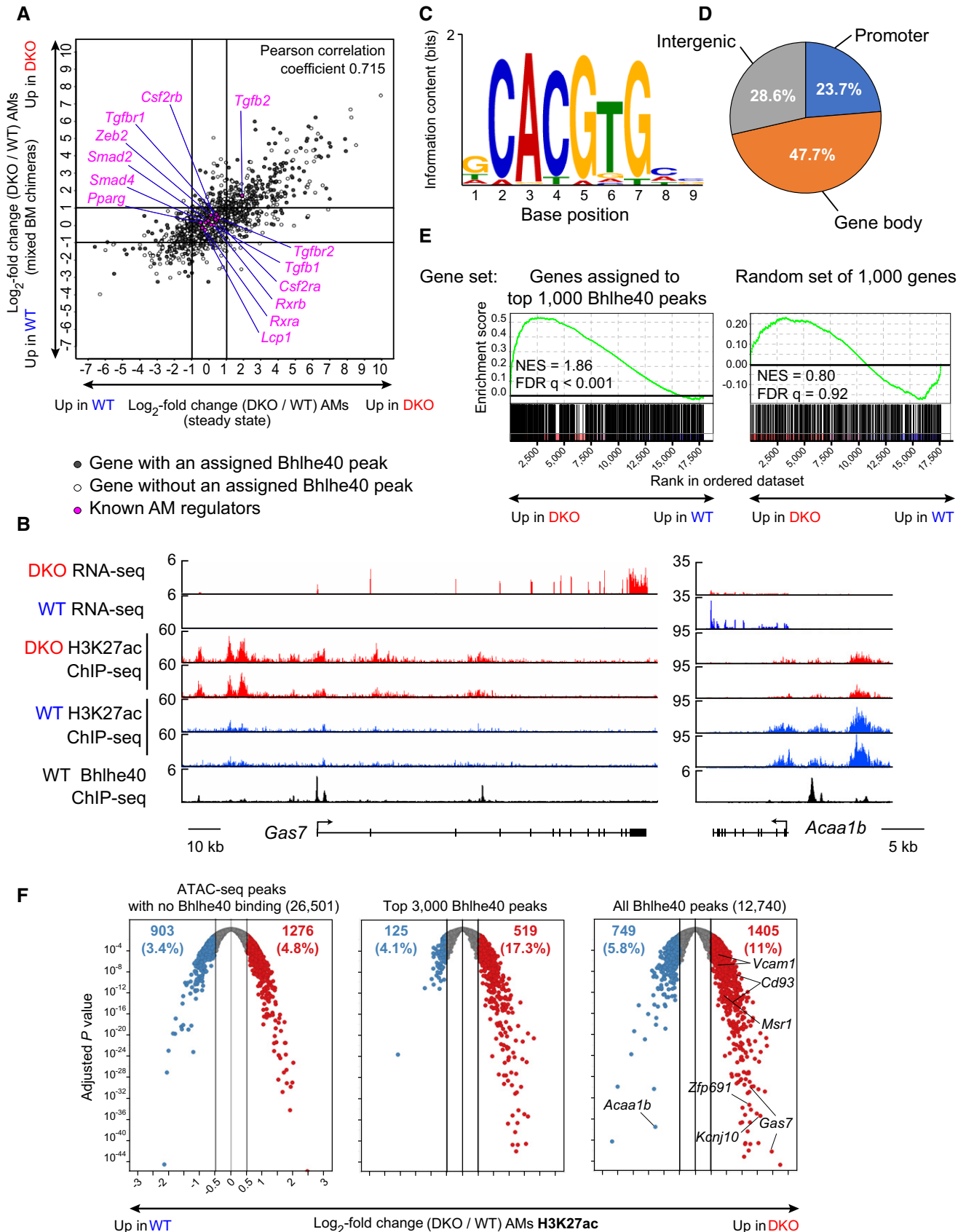


Figure 5.

Figure 5. Genome-wide analysis of Bhlhe40 and Bhlhe41 function in AMs.

- A Comparison of changes in gene expression induced by Bhlhe40/Bhlhe41 deficiency in steady-state knockout mice (horizontal axis) and in mixed BM chimeras (vertical axis). Log₂-transformed DKO/WT fold changes are plotted. Genes with expression of > 5 TPM in at least one of the samples are displayed. Genes highlighted in magenta indicate known and putative regulators of AMs. Closed symbols—Bhlhe40-bound genes (Bhlhe40 ChIP-seq peak assigned to the nearest gene within a 50 kb window). Open symbols—genes without Bhlhe40 binding.
- B Presence of RNA transcripts (RNA-seq; top) at the *Gas7* and *Acaa1b* genes in WT and DKO AMs; the ChIP-seq analysis of H3K27 acetylation in WT and DKO AMs (middle) and Bhlhe40 binding in WT and DKO AMs (bottom). All analyses performed with *ex vivo* AMs.
- C Consensus Bhlhe40-binding motif identified by *de novo* motif discovery (MEME-ChIP suite; *E*-value, 8.6×10^{-123}).
- D Distribution of Bhlhe40 peaks at intergenic regions, the gene body or the promoter in AMs.
- E Gene set enrichment analysis (GSEA) on dataset ranked by DKO/WT fold change in steady-state AM RNA-seq using set of genes assigned to top 1,000 Bhlhe40 peaks (ranked by *P* value) (left) or a random set of 1,000 genes (right). Similar results were obtained with all three random sets tested. NES—normalized enrichment score. FDR—false discovery rate.
- F Pairwise comparison of H3K27 acetylation in WT and DKO AMs performed on 2-kb regions around the Bhlhe40 peak summits [right—for all Bhlhe40 peaks called with *P* value of $< 10^{-10}$; center—for top 3,000 Bhlhe40 peaks (ranked by *P* value)] and around WT AM ATAC-seq peaks (Immgen) that did not have a Bhlhe40 peak in their close proximity (filtered as described in Materials and Methods) (left). Volcano plots show adjusted *P* values (vertical axes) and log₂ fold change (horizontal axes) for H3K27ac pairwise comparison in WT vs. DKO AMs; genes assigned to some of the Bhlhe40-binding regions are labeled on the left plot.

previously defined based on their exclusive expression or exclusive lack of expression, respectively, by AM, when compared to other tissue-resident macrophage populations (Gautier *et al*, 2012b; Schneider *et al*, 2014). Strikingly, most of the “non-AM macrophage signature” genes were upregulated in DKO AMs, while many genes from the “AM signature” showed the opposite trend, albeit to a lesser degree (Figs 6A and EV5A). Both changes—the upregulation of “non-AM macrophage signature” and the downregulation of the “AM signature”—were significant when compared to the total number of upregulated or downregulated genes in DKO macrophages, respectively ($P < 0.0001$, Fisher’s exact test). These changes included the downregulation of genes encoding the AM-specific adhesion molecule EPCAM (*Epcam*) and acetyl-coenzyme A acyl-transferase 1B (*Acaa1b*), which is involved in lipid metabolism, as well as the upregulation of genes that are broadly expressed by tissue-resident macrophage populations other than AMs, including those encoding the complement component C1q (*C1qa*, *C1qb*, *C1qc*), transcription factor MafB (*Mafb*), cholesterol carrier apolipoprotein E (*ApoE*), and chemokine-like receptor 1 (*Cnklr1*) (Fig 6A).

The dysregulation of the AM signature genes, the upregulation of AM lineage-inappropriate genes, and the accumulation of lipid droplets in DKO AMs were reminiscent of the phenotype observed in PPAR γ -deficient AMs (Baker *et al*, 2010; Gautier *et al*, 2012a; Schneider *et al*, 2014). While *Cd11c*-Cre *Pparg*^{fl/fl} AMs also failed to acquire a mature Siglec F⁺ CD11b^{lo/int} cell-surface phenotype (Schneider *et al*, 2014), a defect that was not observed in DKO mice, we nevertheless compared the transcriptome changes resulting from Bhlhe40/Bhlhe41 deficiency with those previously described for PPAR γ -deficient AMs (Schneider *et al*, 2014). Unexpectedly, despite normal expression of *Pparg* by DKO AMs (Fig 5A) and normal expression of *Bhlhe40* and *Bhlhe41* by *Cd11c*-Cre *Pparg*^{fl/fl} AMs (Fig EV3C), this analysis revealed striking similarities in the transcriptome changes observed in these two mutant AMs (Fig EV5B). This overlap was particularly pronounced for genes co-repressed by PPAR γ and Bhlhe40/Bhlhe41 and was less evident for activated genes (Fig EV5B). The expression changes of PPAR γ -regulated genes in the DKO cells were cell-intrinsic as they were also observed in mixed BM chimeras (Fig EV5B). Many of the co-regulated genes exhibited Bhlhe40 binding in their proximity, suggesting that they may be directly regulated by Bhlhe40 (Fig EV5B–D). In the absence

of published PPAR γ -binding data for AMs, we utilized the existing PPAR γ ChIP-seq dataset for thioglycollate-elicited peritoneal macrophages to determine possible direct targets of this factor in myeloid cells (Menéndez-Gutiérrez *et al*, 2015). From all of the AM-expressed genes (TPM > 5), 36% exhibited PPAR γ binding in their proximity in thioglycollate-elicited peritoneal macrophages (Fig EV5C). This frequency increased to 53% for the genes that were repressed by PPAR γ in AMs (Schneider *et al*, 2014) and further went up to 78% for the direct Bhlhe40 target genes that were co-repressed by Bhlhe40/Bhlhe41 and PPAR γ (Fig EV5C). Analysis of individual genes suggested that PPAR γ and Bhlhe40 bind to overlapping but distinct sets of regulatory elements in the proximity of the co-regulated genes (Fig EV5D). While direct assessment of genome-wide PPAR γ binding in AMs is desirable in the future, these results suggest that Bhlhe40/Bhlhe41 and PPAR γ regulate overlapping parts of the AM transcriptional program and that this co-regulation may occur through direct binding of these transcription factors to regulatory elements of the common target genes.

Upregulation of the AM lineage-inappropriate genes by DKO AMs prompted us to assess the expression of signatures characteristic for other tissue-resident macrophage populations. Strikingly, signature genes for red pulp macrophages, peritoneal macrophages, and, to a lesser extent, microglia were upregulated in DKO AMs both in the steady state and in mixed BM chimera setting (Figs 6A and EV5A). All of these changes were statistically significant when compared to the total number of genes upregulated in DKO macrophages ($P < 0.0001$, Fisher’s exact test for all three signatures). The upregulated genes included those encoding transcription factors [*Sox4* and *Zfp691* expressed by microglia; *Spic*, encoding a master regulator of red pulp macrophages (Kohyama *et al*, 2008); *Ahr*, *Maf* and *Mafb* more broadly expressed by macrophages and included in the red pulp macrophages signature (Gautier *et al*, 2012b)], surface receptors (*Cd93* and *Msr1*, expressed by peritoneal macrophages, and *Vcam1*, a marker for red pulp macrophages), components of the complement and coagulation cascades (*C4b* and *F13a1*, part of peritoneal macrophage signature), and other genes (Fig 6A). Many of these genes, including *Ahr*, *Spic*, *Vcam1*, *Msr1*, *Cd93*, *Sox4*, and *Zfp691*, had detectable Bhlhe40 binding in their proximity (Figs 5B and 6A, and EV4A) suggesting that Bhlhe40 and Bhlhe41 in WT AMs may directly repress their expression. Interestingly, gene set enrichment analysis showed that DKO peritoneal macrophages

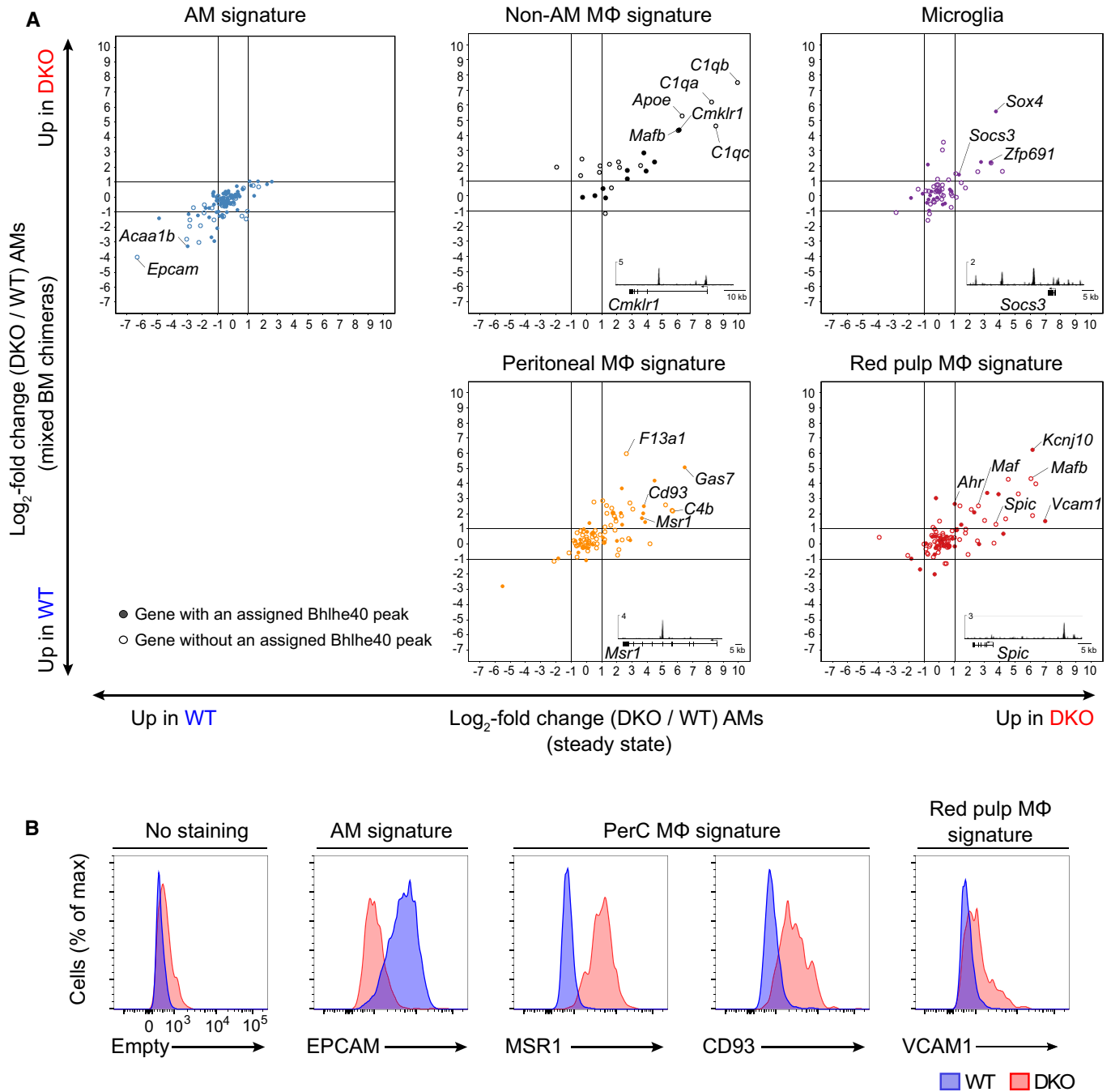


Figure 6. Repression of AM lineage-inappropriate genes by Bhlhe40 and Bhlhe41.

A Comparison of changes in gene expression induced by Bhlhe40/Bhlhe41 deficiency in steady-state knockout mice (horizontal axis) and in mixed BM chimeras (vertical axis) as shown in Fig 5A, but filtered for the indicated signatures (no TPM filter applied). Closed symbols—genes with associated Bhlhe40 binding (as in Fig 5A) revealed by ChIP-seq. Open symbols—genes without Bhlhe40 binding. Insets show Bhlhe40 ChIP-seq track for selected dysregulated genes.

B Flow cytometric comparison of expression of the indicated cell-surface markers (identified in panel A) on WT and DKO AMs. A narrow forward/side scatter gate was applied to correct for possible differences in autofluorescence. Representative results of two independent experiments with three and four mice per group.

likewise downregulated AM signature genes and upregulated red pulp macrophage signature genes, while expression of microglia signature did not show a unidirectional trend in these cells (Fig EV5A). These results suggested that low levels of some AM

signature genes are expressed by peritoneal macrophages in a Bhlhe40-dependent manner and indicated that Bhlhe40/Bhlhe41 may play a role in the repression of a part of the red pulp macrophage program across different tissue-resident macrophage subsets.

The RNA-seq experiments described above could not discriminate if these lineage-inappropriate genes were induced in all DKO AMs or only in a small subset. We therefore next took advantage of the fact that a number of the dysregulated genes encode cell-surface molecules and assessed expression of their corresponding proteins at the single-cell level by flow cytometry. We confirmed the downregulation of the adhesion molecule EPCAM (AM signature), the upregulation of the scavenger receptor *Msr1* and C-type lectin CD93 (peritoneal macrophage signature), as well as the upregulation of VCAM1 (red pulp macrophage signature) in DKO AMs. Importantly, most of these alterations in cell-surface phenotype occurred in the majority of the DKO AMs (Fig 6B). Thus, despite normal expression of the commonly used AM markers, the broad dysregulation of gene expression in DKO AMs was also reflected by alterations in their cell-surface phenotype. Taken together, these results demonstrate that the transcription factors Bhlhe40 and Bhlhe41 are required for the expression of a subset of the AM signature genes, while repressing a surprisingly broad spectrum of genes normally expressed by other macrophage lineages. ChIP-seq results indicate that many of these changes may be explained by direct repression of these genes by Bhlhe40/Bhlhe41.

Discussion

Almost all tissues possess resident populations of phagocytes that have both generic and tissue-specific functions. This dual functionality of tissue-resident macrophages at the molecular level is reflected by the existence of a core macrophage gene expression program (Gautier *et al*, 2012b; Mass *et al*, 2016) controlled by broadly expressed macrophage lineage-defining transcription factors such as PU.1 and C/EBP family members, that is overlaid by tissue-specific programs that are activated by the tissue microenvironment through induction of tissue-specific transcription factors (Okabe & Medzhitov, 2015). In recent years, a number of such factors that regulate the differentiation of tissue-resident macrophage subsets were identified. Among others, this includes LXR α that controls macrophage development in the marginal zone of the spleen (A-Gonzalez *et al*, 2013), PPAR γ , which is crucial for the differentiation of AMs (Schneider *et al*, 2014), Spi-C that regulates red pulp macrophage development (Kohyama *et al*, 2008), and GATA6 that orchestrates the peritoneal macrophage gene expression program (Gautier *et al*, 2014; Okabe & Medzhitov, 2014; Rosas *et al*, 2014). Of note, in many cases there is no simple one-to-one relationship between a macrophage subset and a transcription factor. For example, LXR α regulates marginal zone and metallophilic macrophages in the spleen and Kupffer cells in the liver (A-Gonzalez *et al*, 2013; Scott *et al*, 2018), and PPAR γ is highly expressed by both AMs and red pulp macrophages (Gautier *et al*, 2012a,b). Therefore, the unique tissue-specific identities of macrophage subsets are likely to be controlled by a combinatorial action of multiple transcription factors, some of which may be expressed more broadly than the others. In line with this notion, it was recently reported that the widely expressed transcription factor Zeb2 controls subset-specific molecular programs in AMs, microglia, Kupffer cells, and splenic and colonic macrophages (Scott *et al*, 2018).

Here, we identified the two closely related transcription factors, Bhlhe40 and Bhlhe41, as novel regulators of tissue-resident

macrophages. These factors are expressed by several macrophage populations but are not required for the maintenance of their numbers at the steady state. However, in a competitive setting, the absence of these factors resulted in a severe disadvantage for alveolar and peritoneal macrophages and, on the contrary, positively affected red pulp macrophage numbers. A recent report addressed the role of Bhlhe40 in the regulation of peritoneal macrophage self-renewal (Jarjour *et al*, 2019). In this study, we focused our attention on the role of both Bhlhe40 and Bhlhe41 in AMs—a population that exhibited the strongest dependency on these regulators. Bhlhe40 and Bhlhe41 were required to maintain a normal rate of the self-renewal-associated proliferation in AMs, which was likely achieved through indirect repression of *Maf* and *Mafb*. Repression of *Maf* and *Mafb* by Bhlhe40 is also thought to regulate self-renewal of peritoneal macrophages (Jarjour *et al*, 2019), suggesting that this mechanism is conserved for both macrophage populations. The self-renewal defect of Bhlhe40/Bhlhe41-deficient AMs resulted in a severe competitive disadvantage of these cells evident both in mixed BM chimeras and in experiments with intranasal transfers of AM precursors into neonatal recipients. Taken together, these results indicate that Bhlhe40 and Bhlhe41 are required for the competitive fitness of AMs that are generated both by fetal and adult hematopoiesis. In addition to the self-renewal defect, AMs exhibited a very broad cell-intrinsic transcriptional footprint of Bhlhe40/Bhlhe41 deficiency, associated with upregulation of numerous genes that are normally expressed by macrophage subsets other than AMs.

A broad dysregulation of the AM molecular program was also reported previously for AMs deficient for the transcription factors PPAR γ (Schneider *et al*, 2014), Zeb2 (Scott *et al*, 2018), and Bach2 (Nakamura *et al*, 2013), although, in the latter case, cell-intrinsic and cell-extrinsic aspects of the changes in the expression program remain to be fully understood (Ebina-Shibuya *et al*, 2017). Together with this report, these studies highlight a remarkable complexity of the transcription factor network controlling the AM molecular program. Recent studies demonstrated that tissue-specific molecular programs of resident macrophages, at least in some cases, represent reversible or partially reversible states that require constant instructive signals from the tissue environment for their maintenance, rather than stable differentiation programs. For example, peritoneal macrophages rapidly lose expression of their lineage-defining transcription factor *Gata6* *in vitro* and *in vivo* in the absence of retinoic acid (Gosselin *et al*, 2014). Moreover, while mature peritoneal macrophages failed to fully transdifferentiate into self-renewing AMs upon transfer into the lungs (van de Laar *et al*, 2016), they lost a substantial part of their molecular signature, including expression of *Gata6*, and instead gained expression of approximately 70% of the genes of the AM signature, including the transcription factor PPAR γ (Lavin *et al*, 2014). The plasticity of tissue-resident macrophage programs and their dependence on cell-extrinsic cues suggest that alterations either in signals coming from the tissue microenvironment or in sensing and interpreting these signals by macrophages can result in pronounced distortions in these molecular programs that can be interpreted as “identity loss”.

While in some cases, the loss of identity is manifested by altered expression of “canonical” cell-surface markers, this is not always the case. For example, conditional inactivation of the pan-macrophage transcription factor Zeb2 resulted in profound changes in expression of subset-specific genes in AMs, microglia, Kupffer cells, and

splenic and colonic macrophages, with minor effects on the expression of cell-surface markers usually used to identify these cells (Scott *et al.*, 2018). The same study also demonstrated that loss of the nuclear receptor LXR α also left a broad footprint on the Kupffer cells' transcriptome without affecting numbers and frequency of F4/80⁺CD64⁺ Kupffer cells in the liver. Together with our finding that *Bhlhe40/Bhlhe41* DKO AMs have grossly normal expression of most commonly used AM markers and yet show drastic changes in their transcriptome, these results highlight the importance of genome-wide approaches and/or utilization of broad marker panels in such studies.

The transcriptional programs of tissue-resident macrophages are thought to be induced upon colonization of tissues by cues from local microenvironments (Okabe & Medzhitov, 2015). Indeed, *Bhlhe40* was not expressed by fetal liver monocytes but was upregulated in a fraction of monocytes that colonized fetal lungs. In contrast to this early induction of *Bhlhe40* in AM development, *Bhlhe41* was upregulated only at the late stages of AM differentiation in cells acquiring a mature AM phenotype. Activation of TGF- β signaling in developing AMs may contribute to *Bhlhe40* upregulation as both *Bhlhe40* and *Bhlhe41* were downregulated upon partial inactivation of this pathway in AMs (Yu *et al.*, 2017) and, as we report here, expression of *Bhlhe40* was enhanced by TGF- β in cultured fetal liver monocytes. This observation is in line with previous reports on the role of TGF- β signaling in activating *Bhlhe41* and *Bhlhe40* in a variety of non-hematopoietic cell types (Kato *et al.*, 2014).

We first identified the transcription factors *Bhlhe41* and *Bhlhe40* as regulators of the development and self-renewal of fetal-derived innate-like B-1a cells (Kreslavsky *et al.*, 2017). The results reported here indicate that these factors are important regulators of another self-renewing tissue-resident leukocyte population—AMs. While the *Bhlhe40/Bhlhe41* deficiency resulted in a severe competitive disadvantage for both cell types in mixed BM chimeras, the functions of these factors in the two cell types are different. *Bhlhe40/Bhlhe41*-deficient B-1a cells exhibited impaired pro-survival cytokine signaling due to downregulation of genes encoding subunits of IL-5/IL-3/GM-CSF receptor family, including *Csf2rb* (Kreslavsky *et al.*, 2017), while no such downregulation was observed in DKO AMs. On the contrary, while DKO B-1a cells, despite reduced numbers, exhibited increased proliferation, the proliferation of DKO AMs was impaired, which likely contributed to their competitive disadvantage in chimeric mice. Thus, the regulation of self-renewal of B-1a cells and AMs by *Bhlhe40* and *Bhlhe41* is caused by distinct cell type-specific mechanisms.

Materials and Methods

Mice

All mice used in this study were maintained on the C57BL/6 genetic background. The *Bhlhe41*^{-/-} mice (Rossner *et al.*, 2008), *Bhlhe40*^{-/-} mice (Sun *et al.*, 2001), and *Csf2rb*^{-/-}*Csf2rb2*^{-/-} mice (Scott *et al.*, 2000) were described previously. B6.SJL and F1 progeny of C57BL/6J and B6.SJL were used as WT donors and recipients, respectively, for mixed BM chimera generation. Mice analyzed in this study were at least 7 weeks old, unless stated otherwise. Mice were bred and maintained at the animal facility of the Research Institute for

Molecular Pathology (Vienna, Austria) or at Comparative Medicine Biomedicum facility of Karolinska Institutet (Stockholm, Sweden). All animal experiments were carried out according to valid project licenses, which were approved and regularly controlled by the Austrian and/or Swedish Veterinary Authorities.

Antibodies

Monoclonal antibodies specific for CD11c (N418), CD11b (M1/70), SiglecF (E50-2440), MHC class II (I-A/I-E; M5/114.15.2), F4/80 (F4/80 and BM8), TIM-4 (54 (RMT4-54)), EpCAM (REA977), MSR1 (REA148), CD93 (AA4.1), VCAM-1 (REA971), Ly6C (HK1.4), CD115 (AFS98), Gr-1 (RB6-8C5), CD117/c-Kit (2B8), Sca-1 (D7), CD34 (MEC14.7 and RAM34), CD16/CD32 (93) CD45.1 (A20), CD45.2 (104) were purchased from BD Biosciences, Thermo Fisher Scientific, BioLegend, or Miltenyi Biotec and were used at a dilution of 1:200 or as specified by the manufacturer. In addition, the following antibodies from the same manufacturers were used in “lineage” mix for LSK and CMP identification: CD4 (GK1.5), CD8 α (53-6.7), CD11b (M1/70), CD11c (N418 or HL3), CD19 (6D5 and 1D3), Gr-1 (RB6-8C5), NK1.1 (PK136), TCR β (H57-597), TCR $\gamma\delta$ (GL3), Ter119 (Ter119).

Definition of cell types by flow cytometry

Leukocyte populations, unless stated otherwise, were gated as follows: Lin⁻Sca-1⁺c-Kit⁺ (LSK) cells (CD4⁻CD8⁻TCR β ⁻TCR $\gamma\delta$ ⁻NK1.1⁻CD19⁻CD11b⁻CD11c⁻Gr-1⁻Ter119⁻c-Kit⁺Sca-1⁺), common myeloid progenitors (CMP) (Lin⁻ (as for LSK), c-Kit⁺Sca-1⁻CD34⁺CD16/CD32^{lo}), microglia (CD45^{int}CD11b⁺), Kupffer cells (CD11b⁺F4/80⁺), red pulp macrophages (CD11b^{lo}F4/80^{hi}), alveolar macrophages (CD11c⁺CD11b^{lo/int}SiglecF⁺), F4/80^{lo} small peritoneal macrophages (CD11b⁺MHCII^{hi}F4/80^{lo}), F4/80^{hi} large peritoneal macrophages (CD11b⁺MHCII^{lo}F4/80^{hi} with additional gating on TIM-4⁺ cells when indicated).

Flow cytometry was performed on LSR Fortessa and FACSCanto instruments (BD Biosciences), and sorting was performed on a FACSARIA III (BD Biosciences) or Sony SH800 (Sony Biotechnology) cell sorter. Data were analyzed using FlowJo software (Treestar).

Tissue processing for the analysis of resident macrophages

For red pulp macrophage, Kupffer cell, AM, and microglia analyses, spleens, livers, lungs, and brains, respectively, were cut into small pieces with scissors and digested with 1 mg/ml collagenase type 4 (Worthington) and 33.3 unit/ml DNase I (Sigma-Aldrich) in IMDM medium for 45–60 min at 37°C with shaking. After digestion, single-cell suspensions were obtained by pipetting and mechanical dissociation of the remaining pieces through cell strainers (BD Falcon). Microglia was further purified by centrifugation in 36% Percoll (20 min, room temperature, 800 g, without brakes). Livers were perfused with PBS prior to harvest to minimize blood contamination. In some experiments (where indicated), AMs were isolated from BAL fluid that was obtained by insertion of a blunt needle into a cut in the trachea and flushing lungs eight times with 500 μ l of ice-cold PBS with 5 mM EDTA. Peritoneal cells were isolated by peritoneal lavage performed with 10 ml of FACS buffer [PBS with 2% fetal calf serum (FCS)].

Generation of mixed BM chimeras

BM cells from WT (B6.SJL, CD45.1) and *Bhlhe40*^{-/-}, *Bhlhe41*^{-/-}, or *Bhlhe40*^{-/-}*Bhlhe41*^{-/-} mice (CD45.2) were stained with CD4, CD8, TCR β , TCR $\gamma\delta$, NK1.1, CD19, CD11b, CD11c, Gr-1, and Ter119 PE-labeled antibodies followed by magnetic depletion with anti-PE MicroBeads (Miltenyi Biotec). WT and DKO cells were mixed at a 1:1 or 1:20 ratio (as indicated), and 2×10^6 cells were transferred intravenously into lethally irradiated (split dose—500 rads, twice) CD45.1/CD45.2 heterozygous (C57BL/6J \times B6.SJL F1) recipients. Chimeras were analyzed > 6 weeks after reconstitution.

For establishment of lung-shielded BM chimeras, C57BL/6J \times B6.SJL F1 recipients were anesthetized with isoflurane and the lung was protected from irradiation using custom-made lead shields, covering the upper part of the abdomen. Mice were irradiated (single dose—1,000 rad), a single dose of busulfan (20 mg/kg body weight) was injected intraperitoneally 6 h later followed by transfer of lineage-depleted BM cells 12 h after injection of busulfan as described above for regular BM chimeras.

Intranasal transfers

For competitive reconstitution of *Csf2rb*^{-/-}*Csf2rb2*^{-/-} mice, CD45⁺CD11b⁺F4/80^{int} fetal monocytes were sorted from the livers of E18.5 WT (CD45.1/.2) and DKO (CD45.2) embryos. Neonatal P1–P2 *Csf2rb*^{-/-}*Csf2rb2*^{-/-} recipient mice were anesthetized with isoflurane, and a mixture of 5×10^4 fetal monocytes for each genotype was administered intranasally in 10 μ l PBS.

For transfers into neonatal WT and DKO mice, CD45⁺ cells were sorted from lungs of P1 WT (CD45.1 or CD45.1/.2) mice and 1×10^5 cells were transferred as described above for fetal liver monocytes into WT (CD45.1/.2) or DKO (CD45.2) P1–P2 recipient mice. Recipients were analyzed > 7 weeks after the transfer.

In vitro measurement of AM proliferation and survival

CD11c⁺CD11b^{lo/int}Siglec F⁺ AMs were sorted from digested lungs of WT (CD45.1) and DKO (CD45.2) mice, mixed in 1:1 ratio, labeled with CellTrace Violet (1 μ M, labeling was performed in 0.1% BSA in PBS solution for 7 min at 37°C), and cultured in RPMI medium containing 10% FCS, 25 mM HEPES, 1 mM L-glutamine, 1 mM sodium pyruvate, and 50 μ M β -mercaptoethanol in the presence of 30 ng/ml of recombinant GM-CSF (PeproTech). CellTrace Violet dilution and ratio of CD45.1⁺ and CD45.2⁺ cells were analyzed immediately after labeling and 7 days after the initiation of the cultures. For assessment of survival, WT and DKO AMs were isolated from BAL fluid by plastic adherence (60 min at 37°C), cultured (WT and DKO cells separately) as described above and stained with Fixable Viability Dye eFluor™780 (Thermo Fisher Scientific) directly on the plate (to prevent detection of cell death events that occurred during harvesting). Supernatant containing few floating cells were also harvested, stained with Fixable Viability Dye, and pooled with the rest of the sample before analysis on flow cytometer.

Culture of fetal monocytes

Fetal monocytes (CD45⁺Ly6G⁻Ly6C⁺CD11b⁺CD64^{int}) were sorted from fetal livers (E15.5) and cultured at 40,000 cells per well in

48-well plates in complete DMEM (PAN Biotech), plus 1 mM Sodium Pyruvate, 1 \times GlutaMAX (Gibco), 10% FCS, 1% Pen/Strep (Gibco), 10 mM HEPES (Gibco) with 50 ng/ml GM-CSF (Biolegend). Cultures were supplemented with either 8.6 mg/ml mouse IgG1 isotype control (MOPC-21, BioXcell), 8.6 mg/ml anti-pan TGF- β 1 antibody (clone: 1D11.16.8, BioXcell), or with 10 ng/ml hTGF- β 1 (PeproTech) for 24 h. Cells were then processed for RNA isolation.

Quantitative RT-PCR (qRT-PCR)

Total RNA was isolated using Quick-RNA MicroPrep Kit (Zymo Research). cDNA was synthesized with M-MLV reverse transcriptase (Invitrogen), and qRT-PCR was performed on a C1000 Touch Thermo Cycler (Bio-Rad) using SYBR Green master mix (Bio-Rad). *Polr2a* was used as a housekeeping gene, and delta Ct method was used for quantification. The following primers were used: Pol2-F CTG GTC CTT CGA ATC CGC ATC, Pol2-R GCT CGA TAC CCT GCA GGG TCA, *Bhlhe40*-F CTC CTA CCC GAA CAT CTC AAA C, *Bhlhe40*-R CCA GAA CCA CTG CTT TTT CC, *Bhlhe41*-F TCG AAA CGG ACA GCC ATT GA, *Bhlhe41*-R GAG CGC TCC CCA TTC TGT AA.

In vivo assessment of cell proliferation by measurement of EdU incorporation

To measure *in vivo* AM proliferation, mice were injected with 1 mg of 5-ethynyl-2'-deoxyuridine (EdU; Sigma-Aldrich or Thermo Fisher Scientific) intravenous three times on three consecutive days. Mice were harvested 1 day after the last injection and EdU incorporation by AMs was measured by flow cytometry using the Click-iT Plus EdU Pacific Blue Flow Cytometry Assay Kit (Thermo Fisher Scientific), following manufacturer's instructions.

RNA flow cytometry

RNA flow cytometry measurement of *Bhlhe40* and *Bhlhe41* expression was performed using the PrimeFlow RNA Assay (Thermo Fisher Scientific) according to the manufacturer's instructions. High-sensitivity Alexa Fluor 647 probes were used for *Bhlhe40* and *Bhlhe41*. Alexa Fluor 647 *Cd8a* probe was used as negative control.

Staining for lipid content

Oil Red O staining was performed on BAL fluid cytopins from WT and DKO mice. Slides were fixed with 4% PFA in PBS for 10 min, washed twice with water (5 min each), placed in absolute propylene glycol for 5 min followed by staining with 0.5% Oil Red O solution in propylene glycol for 10 min at 60°C. Slides were then rinsed with 85% propylene glycol solution for 5 min, washed twice with water (5 min each), counterstained with hematoxylin solution for 30 s, washed with tap water, mounted with aqueous mounting medium, and scanned with a Panoramic FLASH 250 III slide scanner equipped with an Adimec Quartz Q12A180 camera (40 \times objective).

For BODIPY 493/503 staining, cells were stained with antibodies against cell-surface markers, washed with PBS, and incubated in 1 μ g/ml BODIPY 493/503 (Thermo Fisher Scientific) solution in PBS for 15 min at room temperature, washed three times with FACS buffer, and analyzed by flow cytometry.

ELISA for Surfactant Pulmonary Associated Protein D (SP-D)

ELISA for Surfactant Pulmonary Associated Protein D (SP-D) was performed on BAL fluid of WT and DKO mice using Mouse SP-D DuoSet ELISA Kit (R&D Systems) according to the manufacturer's instructions. BAL fluid from *Csf2rb*^{-/-}*Csf2rb2*^{-/-} mice that develop lung proteinosis was used as a positive control.

ChIP-seq analysis of Bhlhe40 binding and H3K27 acetylation

AMs for Bhlhe40 ChIP were isolated from BAL fluid of WT mice by adherence to plastic (60 min at 37°C) and fixed directly on the plates with 1% PFA in PBS in the presence of 1% FCS at room temperature. Fixation was stopped after 10 min by addition of glycine in PBS (final concentration 0.1 M), and cells were harvested with a cell scraper. AM purity was confirmed to be > 95% by flow cytometry. Cells were washed with 0.1 M glycine solution in PBS and frozen. For H3K27ac ChIP, lungs of WT and DKO mice were digested as described above, stained with antibodies against cell-surface markers, and fixed with 1% PFA in PBS in the presence of 1% FCS at room temperature. Fixation was stopped after 10 min by addition of glycine in PBS (final concentration 0.1 M), and CD11c⁺CD11b^{lo/int} Siglec F⁺ AMs were sorted and frozen. ChIP and library preparation was performed as recently described (Gustafsson *et al*, 2019) with minor modifications. 7.5×10^5 (for Bhlhe40) or 1×10^5 (for H3K27Ac) fixed frozen AMs were thawed at room temperature, pelleted and diluted with SDS lysis buffer (50 mM Tris/HCl pH 8, 0.5% SDS, and 10 mM EDTA pH 8). Cells were sonicated using a Bioruptor Plus sonicator (Diagenode). To neutralize the SDS, Triton X-100 was added to a final concentration of 1% along with cOmplete protease inhibitor. Samples were incubated at room temperature for 10 min. For Bhlhe40 ChIP, streptavidin sepharose magnetic beads (GE Healthcare) were used for chromatin “pre-clearing”. For ChIP, 3 µg of rabbit polyclonal anti-Bhlhe40 antibody (Novus Biologicals, NB100-1800, lot C2) or 3 µg of anti-H3K27Ac antibody (Diagenode #C15410196) was added to 10 µl Protein G-coupled Dynabeads (Thermo Fisher Scientific) in PBS with 0.5% BSA and incubated with rotation for 4 h at 4°C. Antibody-coated Dynabeads were washed with PBS with 0.5% FCS and mixed with cell lysate in PCR tubes. Tubes were incubated rotating overnight at 4°C. Immunoprecipitated chromatin was washed with 150 µl of low-salt buffer (50 mM Tris/HCl, 150 mM NaCl, 0.1% SDS, 0.1% sodium deoxycholate, 1% Triton X-100, and 1 mM EDTA), high-salt buffer (50 mM Tris/HCl, 500 mM NaCl, 0.1% SDS, 0.1% sodium deoxycholate, 1% Triton X-100, and 1 mM EDTA) and LiCl buffer (10 mM Tris/HCl, 250 mM LiCl, 0.5% IGEPAL CA-630, 0.5% sodium deoxycholate, and 1 mM EDTA), followed by two washes with TE buffer (10 mM Tris/HCl and 1 mM EDTA) and two washes with ice-cold Tris/HCl pH 8. For tagmentation, bead bound chromatin was resuspended in 30 µl of tagmentation buffer. 1 µl of transposase (Nextera, Illumina) was added, and samples were incubated at 37°C for 10 min followed by two washes with low-salt buffer. Bead bound tagmented chromatin was diluted in 30 µl of water. 15 µl PCR master mix (Nextera, Illumina) and 5 µl indexed amplification primers (Buenrostro *et al*, 2013; 0.125 µM final concentration) were added and libraries prepared using the following PCR program: 72°C 5 min (adapter extension); 95°C 5 min; followed by 11 cycles of 98°C 10 s, 63°C 30 s and 72°C

3 min. All steps from sonication to library amplification PCR were performed in the same PCR tube. A “mock” precipitation sample without antibody but with streptavidin sepharose magnetic beads (GE Healthcare) was processed in parallel to generate the control library. After PCR amplification, library cleanup was done using Agencourt AmPureXP beads (Beckman Coulter) at a PCR mix to bead ratio of 1:1. DNA concentrations in purified samples were measured using the Qubit dsDNA HS Kit (Invitrogen). Libraries were subjected to Illumina deep sequencing (HiSeqV4 SR50 for Bhlhe40 ChIP; NextSeq SR50 for H3K27ac ChIP).

Analysis of ChIP-seq data

For Bhlhe40 ChIP-seq, the reads were aligned to the mouse genome assembly version of July 2007 (NCBI37/mm9), using the Bowtie program version 1.0.0. Peaks were called with a *P* value of $< 10^{-10}$ by using the MACS program version 1.3.6.1 (Feng *et al*, 2012) with default parameters, a genome size of 2,654,911,517 bp (mm9), and a track from the “mock” precipitation described above as a control track. The identified peaks were then assigned to target genes as described (Revilla-i-Domingo *et al*, 2012). Bhlhe40 peaks overlapping with the transcription start site (TSS) were referred to as promoter peaks in Fig 5D. For our H3K27ac ChIP-seq samples and for Immgen AM ATAC-seq sample (GSM2692306) (Yoshida *et al*, 2019), reads were aligned to the mouse genome assembly version of July 2007 (NCBI37/mm9), using the Bowtie2 program (Langmead & Salzberg, 2012) (usegalaxy.eu; galaxy version 2.3.4.2). Peak calling for ATAC-seq was performed as described above for Bhlhe40 ChIP-seq. ATAC-seq peaks that do not have Bhlhe40 peaks in their proximity were identified using Multovl tool version 1.2 using exact borders for called ATAC-seq peaks and regions extending ± 1 kb from peak summits for Bhlhe40 peaks. Peaks with *P* value of $< 10^{-10}$ were used both for ATAC-seq and for Bhlhe40 ChIP-seq in this analysis. The analysis identified 26,501 out of 36,406 ATAC-seq peaks. For H3K27ac pairwise comparison, reads within ± 1 kb regions from ATAC-seq or Bhlhe40 ChIP-seq summits were counted using HTseq version 0.5.3 (Anders *et al*, 2014). The datasets were analyzed using the R package DESeq2 version 1.2.10 (Love *et al*, 2014) using the default DESeq2 settings.

The PPAR γ ChIP-seq dataset for thioglycollate-elicited peritoneal macrophages (Menéndez-Gutiérrez *et al*, 2015; GSM1555714 in GEO database) peak set with a *P* value of $< 10^{-10}$ was obtained from ChIP-Atlas database (SRX769794).

For motif discovery, we used the MEME-ChIP suite (version 4.9.1; Machanick & Bailey, 2011) to predict the most significant motifs present in the 300 bp centered at the peak summit of the top 300 sequences, as sorted by the fold enrichment score of the MACS program.

RNA-seq analysis

RNA-seq experiments were performed on double-sorted CD11c⁺CD11b^{lo/int} Siglec F⁺ AMs and CD11b⁺F4/80⁺MHCII^{int}Tim4⁺ large peritoneal macrophages on steady-state WT and DKO mice as well as on double-sorted CD45.1⁺ WT and CD45.2⁺ DKO CD11c⁺CD11b^{lo/int} Siglec F⁺ AMs from mixed BM chimeras as previously described (Kreslavsky *et al*, 2017) with minor modifications. In brief, RNA was isolated with RNeasy Plus Mini or Micro Kits (Qiagen),

and mRNA was obtained by poly(A) selection with a Dynabeads mRNA purification kit (Thermo Fisher Scientific), followed by fragmentation by heating at 94°C for 3 min (in fragmentation buffer). The fragmented mRNA was used as a template for first-strand cDNA synthesis with random hexamers and a Superscript VILO cDNA Synthesis kit (Thermo Fisher Scientific). The second-strand cDNA was synthesized with 100 mM dATP, dCTP, dGTP, and dUTP in the presence of RNase H, *Escherichia coli* DNA polymerase I and DNA ligase (Thermo Fisher Scientific). Sequencing libraries were prepared with the NEBNext Ultra II DNA Library Prep Kit for Illumina (New England BioLabs). For strand-specific RNA-sequencing, the uridines present in one cDNA strand were digested with uracil-N-glycosylase (New England BioLabs), as described (Parkhomchuk *et al*, 2009), followed by PCR amplification with NEBNext UltraII Q5 Master Mix (New England BioLabs). Libraries were subjected to Illumina deep sequencing (HiSeqV4 SR50). All RNA-seq experiments were performed with two biological replicates.

Bioinformatic analysis of RNA-seq data

Sequence reads that passed the Illumina quality filtering were considered for alignment. Reads corresponding to mouse ribosomal RNAs (BK000964.1 and NR046144.1) were removed. The remaining reads were cut down to a read length of 44 bp and aligned to the mouse transcriptome (genome assembly version of July 2007 NCBI37/mm9) using TopHat version 1.4.1 (Trapnell *et al*, 2009). The calculation of RNA expression values was all based on the RefSeq database, which was downloaded from UCSC on January 10, 2014. The annotation of immunoglobulin and T cell receptor genes was incorporated from the Ensembl release 67 (Cunningham *et al*, 2015). Genes with overlapping exons were flagged, and double entries (i.e. exactly the same gene at two different genomic locations) were renamed. Genes with several transcripts were merged to consensus genes consisting of a union of all underlying exons using the fuge software (I. Tamir, unpublished), which resulted in 25,726 gene models.

For analysis of differential gene expression, the number of reads per gene was counted using HTseq version 0.5.3 (Anders *et al*, 2014) with the overlap resolution mode set to “union”. The datasets were analyzed using the R package DESeq2 version 1.2.10 (Love *et al*, 2014). Sample normalizations and dispersion estimations were conducted using the default DESeq2 settings. Transcripts per million (TPM) were calculated from RNA-seq data, as described (Wagner *et al*, 2012).

GSEA was performed using the GSEA software from the Broad Institute (Subramanian *et al*, 2005). Genes were ranked on the basis of their change in expression (\log_2 fold values) as determined by the DESeq2 package and were compared to gene sets from the MSigDB or defined gene sets from literature. Random gene sets were generated using <http://www.molbiotools.com/randomgenesetgenerator.html> tool.

PPAR γ -regulated AM genes were identified as genes that significantly (adjusted *P* value < 0.05) changed their expression more than twofold in adult PPAR γ -deficient AM samples compared to their WT counterparts [GSE60249 dataset (Schneider *et al*, 2014)] using GEO2R tool. Tissue-resident macrophage gene expression signatures used in this study were described previously (Gautier *et al*, 2012b; Schneider *et al*, 2014).

Statistical analysis

Statistical analysis was performed with the GraphPad Prism 7 software. Statistical significance of differences between two experimental groups in all experiments, with the exception of those involving NGS-based approaches, was assessed by two-tailed Student's *t*-test analysis. The statistical evaluation of the RNA-seq data is described in the section dealing with the bioinformatic analysis of RNA-seq data. Analysis of enrichment in signature genes was performed using Fisher's exact test in GraphPad Prism 7 software; this analysis was focused on the genes that were significantly up- or downregulated over twofold threshold in AMs both in mixed BM chimeras and in steady-state settings.

Data availability

RNA-seq and ChIP-seq data first reported in this study are available at the Gene Expression Omnibus (GEO) repository under the accession number GSE135018 (<https://www.ncbi.nlm.nih.gov/geo/query/acc.cgi?acc=GSE135018>). The following previously published ATAC-seq, ChIP-seq, microarray, and RNA-seq datasets were used in this study: GSM2692306 (<https://www.ncbi.nlm.nih.gov/geo/query/acc.cgi?acc=GSM2692306>) (AM ATAC-seq; GEO), GSM1555714 (<https://www.ncbi.nlm.nih.gov/geo/query/acc.cgi?acc=GSM1555714>) (ChIP-seq for PPAR γ in thioglycollate-elicited peritoneal macrophages; GEO), GSE60249 (<https://www.ncbi.nlm.nih.gov/geo/query/acc.cgi?acc=GSE60249>) (microarray analysis of *Itgax*-Cre *Pparg*^{fl/fl} AMs; GEO), GSE60528 (<https://www.ncbi.nlm.nih.gov/geo/query/acc.cgi?acc=GSE60528>) (microarray analysis of *Csf2rb*^{-/-} AMs; GEO), E-MTAB-6028 (<https://www.ebi.ac.uk/arrayexpress/experiments/E-MTAB-6028/>) (RNA-seq analysis of *Itgax*^{Cre} *Tgfb2*^{fl/fl} AMs; ArrayExpress).

Expanded View for this article is available online.

Acknowledgements

We thank M. Fischer and M. Jaritz for help with bioinformatics analysis; G. Schmauß, M. Weninger and their colleagues for sorting by flow cytometry; A. Sommer's team at the Vienna Biocenter Support Facilities GmbH (VBCF) for Illumina sequencing; J. Klughofer and A. Piszczek for histological service; and R. L. Schenk for proofreading of the manuscript. This study was supported by Boehringer Ingelheim, the Austrian Science Fund (grant P28841 to T.K.), the Austrian Industrial Research Promotion Agency (Headquarter Grant FFG-852936 to M. B.), the Swedish Research Council (grant 2017-01118 to T.K.), Cancerfonden (grant CAN 2018/710 to T.K.), Åke Wibergs Stiftelse (grant M18-0094 to T.K.) and a stipend from Wenner-Gren Foundations (to T.K.). M.H.S. was supported by grants from the Agence Nationale de la Recherche (ANR-11-BSV3-0026), Fondation pour la Recherche Médicale (DEQ. 20110421320), the European Research Council (ERC) under the European Union's Horizon 2020 research and innovation program (grant agreement number 695093 MacAge). A.R. was supported by a stipend from the German Research Foundation DFG (RE 4264/1-1).

Author contributions

RR performed most of the experiments; TK and MB supervised the study; CG, RM and TK performed the ChIP-seq experiments; AR performed RNA flow cytometry on stages of alveolar macrophage development and *in vitro* survival

experiments; TK performed RNA-seq library preparation; DC and MG analyzed Bhlhe40 induction by TGF- β 1; RT and MJR provided knockout mouse strains; LT suggested the study and participated in the initial experiments; NA-G, MHS and SS provided crucial expertise on macrophage biology and performed experiments that were not included in the final version of the manuscript; TK wrote the manuscript; RR, CG, NA-G, LT, MS, RM, and MB edited the manuscript.

Conflict of interest

The authors declare that they have no conflict of interest.

References

- A-Gonzalez N, Guillen JA, Gallardo G, Diaz M, de la Rosa JV, Hernandez IH, Casanova-Acebes M, Lopez F, Tabraue C, Beceiro S *et al* (2013) The nuclear receptor LXR α controls the functional specialization of splenic macrophages. *Nat Immunol* 14: 831
- Amit I, Winter DR, Jung S (2015) The role of the local environment and epigenetics in shaping macrophage identity and their effect on tissue homeostasis. *Nat Immunol* 17: 18
- Anders S, Pyl PT, Huber W (2014) HTSeq—a Python framework to work with high-throughput sequencing data. *Bioinformatics* 31: 166–169
- Aziz A, Soucie E, Sarrazin S, Sieweke MH (2009) MafB/c-Maf deficiency enables self-renewal of differentiated functional macrophages. *Science* 326: 867–871
- Bain CC, Bravo-Blas A, Scott CL, Gomez Perdiguero E, Geissmann F, Henri S, Malissen B, Osborne LC, Artis D, Mowat AM (2014) Constant replenishment from circulating monocytes maintains the macrophage pool in the intestine of adult mice. *Nat Immunol* 15: 929
- Bain CC, Hawley CA, Garner H, Scott CL, Schridde A, Steers NJ, Mack M, Joshi A, Guillems M, Mowat AM (2016) Long-lived self-renewing bone marrow-derived macrophages displace embryo-derived cells to inhabit adult serous cavities. *Nat Commun* 7: ncomms11852
- Baker AD, Malur A, Barna BP, Ghosh S, Kavuru MS, Malur AG, Thomassen MJ (2010) Targeted PPAR γ deficiency in alveolar macrophages disrupts surfactant catabolism. *J Lipid Res* 51: 1325–1331
- Bonfield TL, Farver CF, Barna BP, Malur A, Abraham S, Raychaudhuri B, Kavuru MS, Thomassen MJ (2003) Peroxisome proliferator-activated receptor- γ is deficient in alveolar macrophages from patients with alveolar proteinosis. *Am J Respir Cell Mol Biol* 29: 677–682
- Buenrostro JD, Giresi PG, Zaba LC, Chang HY, Greenleaf WJ (2013) Transposition of native chromatin for fast and sensitive epigenomic profiling of open chromatin, DNA-binding proteins and nucleosome position. *Nat Methods* 10: 1213
- Cunningham F, Amode MR, Barrell D, Beal K, Billis K, Brent S, Carvalho-Silva D, Clapham P, Coates G, Fitzgerald S (2015) Ensembl 2015. *Nucleic Acids Res* 43: D662–D669
- Dranoff G, Crawford A, Sadelain M, Ream B, Rashid A, Bronson R, Dickersin G, Bachurski C, Mark E, Whittsett J *et al* (1994) Involvement of granulocyte-macrophage colony-stimulating factor in pulmonary homeostasis. *Science* 264: 713–716
- Ebina-Shibuya R, Matsumoto M, Kuwahara M, Jang K-J, Sugai M, Ito Y, Funayama R, Nakayama K, Sato Y, Ishii N *et al* (2017) Inflammatory responses induce an identity crisis of alveolar macrophages, leading to pulmonary alveolar proteinosis. *J Biol Chem* 292: 18098–18112
- Feng J, Liu T, Qin B, Zhang Y, Liu XS (2012) Identifying ChIP-seq enrichment using MACS. *Nat Protoc* 7: 1728
- Garbi N, Lambrecht BN (2017) Location, function, and ontogeny of pulmonary macrophages during the steady state. *Pflügers Arch Eur J Physiol* 469: 561–572
- Garriga-Canut M, Roopra A, Buckley NJ (2001) The basic helix-loop-helix protein, SHARP-1, represses transcription by a histone deacetylase-dependent and histone deacetylase-independent mechanism. *J Biol Chem* 276: 14821–14828
- Gautier EL, Chow A, Spanbroek R, Marcelin G, Greter M, Jakubzick C, Bogunovic M, Leboeuf M, van Rooijen N, Habenicht AJ *et al* (2012a) Systemic analysis of PPAR γ in mouse macrophage populations reveals marked diversity in expression with critical roles in resolution of inflammation and airway immunity. *J Immunol* 189: 2614–2624
- Gautier EL, Shay T, Miller J, Greter M, Jakubzick C, Ivanov S, Helft J, Chow A, Elpek KG, Gordonov S *et al* (2012b) Gene-expression profiles and transcriptional regulatory pathways that underlie the identity and diversity of mouse tissue macrophages. *Nat Immunol* 13: 1118
- Gautier EL, Ivanov S, Williams JW, Huang SC-C, Marcelin G, Fairfax K, Wang PL, Francis JS, Leone P, Wilson DB *et al* (2014) Gata6 regulates aspartoacylase expression in resident peritoneal macrophages and controls their survival. *J Exp Med* 211: 1525–1531
- Ginhoux F, Greter M, Leboeuf M, Nandi S, See P, Gokhan S, Mehler MF, Conway SJ, Ng LG, Stanley ER *et al* (2010) Fate mapping analysis reveals that adult microglia derive from primitive macrophages. *Science* 330: 841–845
- Ginhoux F, Guillems M (2016) Tissue-resident macrophage ontogeny and homeostasis. *Immunity* 44: 439–449
- Gomez Perdiguero E, Klapproth K, Schulz C, Busch K, Azzoni E, Crozet L, Garner H, Trouillet C, de Bruijn MF, Geissmann F *et al* (2014) Tissue-resident macrophages originate from yolk-sac-derived erythro-myeloid progenitors. *Nature* 518: 547
- Gosselin D, Link VM, Romanoski Casey E, Fonseca Gregory J, Eichenfield Dawn Z, Spann Nathanael J, Stender Joshua D, Chun Hyun B, Garner H, Geissmann F *et al* (2014) Environment drives selection and function of enhancers controlling tissue-specific macrophage identities. *Cell* 159: 1327–1340
- Guillems M, De Kleer I, Henri S, Post S, Vanhoutte L, De Prijck S, Deswarte K, Malissen B, Hammad H, Lambrecht BN (2013) Alveolar macrophages develop from fetal monocytes that differentiate into long-lived cells in the first week of life via GM-CSF. *J Exp Med* 210: 1977–1992
- Gustafsson C, De Paepe A, Schmidl C, Mansson R (2019) High-throughput ChIPmentation: freely scalable, single day ChIPseq data generation from very low cell-numbers. *BMC Genomics* 20: 59
- Hashimoto D, Chow A, Noizat C, Teo P, Beasley Mary B, Leboeuf M, Becker Christian D, See P, Price J, Lucas D *et al* (2013) Tissue-resident macrophages self-maintain locally throughout adult life with minimal contribution from circulating monocytes. *Immunity* 38: 792–804
- Heng TS, Painter MW (2008) The Immunological Genome Project: networks of gene expression in immune cells. *Nat Immunol* 9: 1091–1094
- Hoeffel G, Wang Y, Greter M, See P, Teo P, Malleret B, Leboeuf M, Low D, Oller G, Almeida F *et al* (2012) Adult Langerhans cells derive predominantly from embryonic fetal liver monocytes with a minor contribution of yolk sac-derived macrophages. *J Exp Med* 209: 1167–1181
- Huang DW, Sherman BT, Lempicki RA (2008) Systematic and integrative analysis of large gene lists using DAVID bioinformatics resources. *Nat Protoc* 4: 44–57
- Hubbard LL, Ballinger MN, Wilke CA, Moore BB (2008) Comparison of conditioning regimens for alveolar macrophage reconstitution and innate immune function post bone marrow transplant. *Exp Lung Res* 34: 263–275

- Jarjour NN, Schwarzkopf EA, Bradstreet TR, Shchukina I, Lin C-C, Huang SC-C, Lai C-W, Cook ME, Taneja R, Stappenbeck TS et al (2019) Bhlhe40 mediates tissue-specific control of macrophage proliferation in homeostasis and type 2 immunity. *Nat Immunol* 20: 687–700
- Jolma A, Yan J, Whittington T, Toivonen J, Nitta Kazuhiro R, Rastas P, Morgunova E, Enge M, Taipale M, Wei G et al (2013) DNA-binding specificities of human transcription factors. *Cell* 152: 327–339
- Kato Y, Kawamoto T, Fujimoto K, Noshiro M (2014) DEC1/STRA13/SHARP2 and DEC2/SHARP1 coordinate physiological processes, including circadian rhythms in response to environmental stimuli. *Curr Top Dev Biol* 110: 339–372
- Kohyama M, Ise W, Edelson BT, Wilker PR, Hildner K, Mejia C, Frazier WA, Murphy TL, Murphy KM (2008) Role for Spi-C in the development of red pulp macrophages and splenic iron homeostasis. *Nature* 457: 318
- Kreslavsky T, Vilagos B, Tagoh H, Poliakov DK, Schwickert TA, Wohner M, Jaritz M, Weiss S, Taneja R, Rossner MJ et al (2017) Essential role for the transcription factor Bhlhe41 in regulating the development, self-renewal and BCR repertoire of B-1a cells. *Nat Immunol* 18: 442–455
- Kreslavsky T, Wong JB, Fischer M, Skok JA, Busslinger M (2018) Control of B-1a cell development by instructive BCR signaling. *Curr Opin Immunol* 51: 24–31
- van de Laar L, Saelens W, De Prijck S, Martens L, Scott Charlotte L, Van Isterdael G, Hoffmann E, Beyaert R, Saeys Y, Lambrecht Bart N et al (2016) Yolk sac macrophages, fetal liver, and adult monocytes can colonize an empty niche and develop into functional tissue-resident macrophages. *Immunity* 44: 755–768
- Langmead B, Salzberg SL (2012) Fast gapped-read alignment with Bowtie 2. *Nat Methods* 9: 357
- Lavin Y, Winter D, Blecher-Gonen R, David E, Keren-Shaul H, Merad M, Jung S, Amit I (2014) Tissue-resident macrophage enhancer landscapes are shaped by the local microenvironment. *Cell* 159: 1312–1326
- Lavin Y, Mortha A, Rahman A, Merad M (2015) Regulation of macrophage development and function in peripheral tissues. *Nat Rev Immunol* 15: 731
- Love MI, Huber W, Anders S (2014) Moderated estimation of fold change and dispersion for RNA-seq data with DESeq2. *Genome Biol* 15: 550
- Machanic P, Bailey TL (2011) MEME-ChIP: motif analysis of large DNA datasets. *Bioinformatics* 27: 1696–1697
- Mass E, Ballesteros I, Farlik M, Halbritter F, Günther P, Crozet L, Jacome-Galarza CE, Händler K, Klughammer J, Kobayashi Y et al (2016) Specification of tissue-resident macrophages during organogenesis. *Science* 353: aaf4238
- Menéndez-Gutiérrez MP, Rószter T, Fuentes L, Núñez V, Escolano A, Redondo JM, De Clerck N, Metzger D, Valledor AF, Ricote M (2015) Retinoid X receptors orchestrate osteoclast differentiation and postnatal bone remodeling. *J Clin Invest* 125: 809–823
- Merad M, Manz MG, Karsunky H, Wagers A, Peters W, Charo I, Weissman IL, Cyster JG, Engleman EG (2002) Langerhans cells renew in the skin throughout life under steady-state conditions. *Nat Immunol* 3: 1135
- Nakamura A, Ebina-Shibuya R, Itoh-Nakadai A, Muto A, Shima H, Saigusa D, Aoki J, Ebina M, Nukiwa T, Igarashi K (2013) Transcription repressor Bach2 is required for pulmonary surfactant homeostasis and alveolar macrophage function. *J Exp Med* 210: 2191–2204
- Numata A, Kwok HS, Kawasaki A, Li J, Zhou Q-L, Kerry J, Benoukraf T, Bararia D, Li F, Ballabio E et al (2018) The basic helix-loop-helix transcription factor SHARP1 is an oncogenic driver in MLL-AF6 acute myelogenous leukemia. *Nat Commun* 9: 1622
- Okabe Y, Medzhitov R (2014) Tissue-specific signals control reversible program of localization and functional polarization of macrophages. *Cell* 157: 832–844
- Okabe Y, Medzhitov R (2015) Tissue biology perspective on macrophages. *Nat Immunol* 17: 9
- Ow JR, Tan YH, Jin Y, Bahirvani AG, Taneja R (2014) Chapter nine – Stra13 and Sharp-1, the non-grouchy regulators of development and disease. In *Current topics in developmental biology*, Reshma T (ed.), Vol. 110, pp 317–338. Cambridge, MA: Academic Press
- Parkhomchuk D, Borodina T, Amstislavskiy V, Banaru M, Hallen L, Krobitsch S, Lehrach H, Soldatov A (2009) Transcriptome analysis by strand-specific sequencing of complementary DNA. *Nucleic Acids Res* 37: e123
- Perdiguer EG, Geissmann F (2015) The development and maintenance of resident macrophages. *Nat Immunol* 17: 2
- Revilla-i-Domingo R, Bilic I, Vilagos B, Tagoh H, Ebert A, Tamir IM, Smeenk L, Trupke J, Sommer A, Jaritz M et al (2012) The B-cell identity factor Pax5 regulates distinct transcriptional programmes in early and late B lymphopoiesis. *EMBO J* 31: 3130–3146
- Rosas M, Davies LC, Giles PJ, Liao C-T, Kharfan B, Stone TC, O'Donnell VB, Fraser DJ, Jones SA, Taylor PR (2014) The transcription factor gata6 links tissue macrophage phenotype and proliferative renewal. *Science* 344: 645–648
- Rossner MJ, Oster H, Wichert SP, Reinecke L, Wehr MC, Reinecke J, Eichele G, Taneja R, Nave K-A (2008) Disturbed clockwork resetting in Sharp-1 and Sharp-2 single and double mutant mice. *PLoS One* 3: e2762
- Sawai CM, Babovic S, Upadhaya S, Knapp David JHF, Lavin Y, Lau Colleen M, Goloborodko A, Feng J, Fujisaki J, Ding L et al (2016) Hematopoietic stem cells are the major source of multilineage hematopoiesis in adult animals. *Immunity* 45: 597–609
- Schneider C, Nobs SP, Kurrer M, Rehrauer H, Thiele C, Kopf M (2014) Induction of the nuclear receptor PPAR- γ by the cytokine GM-CSF is critical for the differentiation of fetal monocytes into alveolar macrophages. *Nat Immunol* 15: 1026
- Scott CL, Robb L, Papaevangelou B, Mansfield R, Nicola NA, Begley CG (2000) Reassessment of interactions between hematopoietic receptors using common beta-chain and interleukin-3-specific receptor beta-chain-null cells: no evidence of functional interactions with receptors for erythropoietin, granulocyte colony-stimulating factor, or stem cell factor. *Blood* 96: 1588–1590
- Scott CL, Zheng F, De Baetselier P, Martens L, Saeys Y, De Prijck S, Lippens S, Abels C, Schoonooghe S, Raes G et al (2016) Bone marrow-derived monocytes give rise to self-renewing and fully differentiated Kupffer cells. *Nat Commun* 7: 10321
- Scott CL, T'Jonck W, Martens L, Todorov H, Sichien D, Soen B, Bonnardel J, De Prijck S, Vandamme N, Cannoodt R et al (2018) The transcription factor ZEB2 is required to maintain the tissue-specific identities of macrophages. *Immunity* 49: 312–325.e315
- Shahmoradi A, Radyushkin K, Rossner MJ (2015) Enhanced memory consolidation in mice lacking the circadian modulators Sharp1 and -2 caused by elevated Igf2 signaling in the cortex. *Proc Natl Acad Sci USA* 112: E3582–E3589
- Shibata Y, Berclaz P-Y, Chronos ZC, Yoshida M, Whittsett JA, Trapnell BC (2001) GM-CSF regulates alveolar macrophage differentiation and innate immunity in the lung through PU.1. *Immunity* 15: 557–567
- Sieweke MH, Allen JE (2013) Beyond stem cells: self-renewal of differentiated macrophages. *Science* 342: 1242974
- Soucie EL, Weng Z, Geirsdóttir L, Molawi K, Maurizio J, Fenouil R, Mossadegh-Keller N, Gimenez G, VanHille L, Beniazza M et al (2016) Lineage-specific enhancers activate self-renewal genes in macrophages and embryonic stem cells. *Science* 351: aad5510
- Subramanian A, Tamayo P, Mootha VK, Mukherjee S, Ebert BL, Gillette MA, Paulovich A, Pomeroy SL, Golub TR, Lander ES et al (2005) Gene set

- enrichment analysis: a knowledge-based approach for interpreting genome-wide expression profiles. *Proc Natl Acad Sci USA* 102: 15545–15550
- Sun H, Taneja R (2000) Stra13 expression is associated with growth arrest and represses transcription through histone deacetylase (HDAC)-dependent and HDAC-independent mechanisms. *Proc Natl Acad Sci USA* 97: 4058–4063
- Sun H, Lu B, Li RQ, Flavell RA, Taneja R (2001) Defective T cell activation and autoimmune disorder in Stra13-deficient mice. *Nat Immunol* 2: 1040–1047
- Suzuki T, Arumugam P, Sakagami T, Lachmann N, Chalk C, Sallèse A, Abe S, Trapnell C, Carey B, Moritz T et al (2014) Pulmonary macrophage transplantation therapy. *Nature* 514: 450
- Tamoutounour S, Guilliams M, Montanana Sanchis F, Liu H, Terhorst D, Malosse C, Pollet E, Ardouin L, Luche H, Sanchez C et al (2013) Origins and functional specialization of macrophages and of conventional and monocyte-derived dendritic cells in mouse skin. *Immunity* 39: 925–938
- Trapnell C, Pachter L, Salzberg SL (2009) TopHat: discovering splice junctions with RNA-Seq. *Bioinformatics* 25: 1105–1111
- Wagner GP, Kin K, Lynch VJ (2012) Measurement of mRNA abundance using RNA-seq data: RPKM measure is inconsistent among samples. *Theory Biosci* 131: 281–285
- Yoshida H, Lareau CA, Ramirez RN, Rose SA, Maier B, Wroblewska A, Desland F, Chudnovskiy A, Mortha A, Dominguez C et al (2019) The cis-regulatory atlas of the mouse immune system. *Cell* 176: 897–912.e820
- Yu X, Buttgereit A, Lelios I, Utz SG, Cansever D, Becher B, Greter M (2017) The cytokine TGF- β promotes the development and homeostasis of alveolar macrophages. *Immunity* 47: 903–912.e904